PROJECT A: INVESTIGATION OF THE ROLE OF ATYPICAL CHEMOKINE RECEPTORS CCRL1 AND CCRL2 IN ANTIBODY RESPONSES

AND

PROJECT B: THE BATTLE OF THE CARS: CD28 COSTIMULATORY ENDODOMAINS ENDOW T CELLS WITH MORE ROBUST EFFECTOR FUNCTIONS *IN VITRO* COMPARED TO THEIR 4-1BB COUNTERPARTS

By Benjamin George Wiggins

A thesis submitted to the University of Birmingham
for the degree of Master of Research

UNIVERSITY OF BIRMINGHAM

School of Immunity and Infection/
School of Cancer Sciences,
College of Medical and Dental Sciences,
University of Birmingham,
Submitted 14th May 2014

PROJECT A:

INVESTIGATION OF THE ROLE OF ATYPICAL CHEMOKINE RECEPTORS CCRL1 AND CCRL2 IN ANTIBODY RESPONSES

Ben Wiggins – MRes (Masters in Biomedical Research)

Principal Investigator: Dr Kai-Michael Toellner

Supervised by: Sarah Cook, Yang Zhang, Charlie Cook, Jenny Marshall, Laura Garcia Ibanez

21/10/2013 – 26/01/2014

This project is submitted in partial fulfilment of the requirements for the award of the MRes

MRC Centre for Immune Regulation,

Institute of Biomedical Research

School of Immunity and Infection,

Medical School,

University of Birmingham,

MRC Medical Research Council

Acknowledgements:

First and foremost I would like to thank Kai Toellner for giving me guidance, making the project so interesting and helping me to become a better researcher. Thank you to Sarah Cook for teaching me, looking after me and sharing many laughs with me. Lastly, thank you also to Yang Zhang, Charlie Cook, Jenny Marshall, Laura Garcia Ibanez, Tom Müller, and Ciaran Mooney for answering my questions and making the lab such a fun, friendly place to work.

Table of Contents:

List of Figures and Tables:

ABSTRACT:

CC-Chemokine receptor-like 1 (CCRL1) and 2 (CCRL2) are members of the atypical chemokine receptor family that are defined by the inability to initiate canonical GPCR signalling. CCRL1 has been proposed to be involved in germinal centre maintenance, while CCRL2 is thought to be involved in plasma cell function, however their exact roles are still unclear. Given their close chromosomal locations, it is possible that these genes arose by recent gene duplication and thus have some overlapping function. Therefore this study aimed to investigate the antibody responses in mice doubly deficient in CCRL1 and CCRL2. Double knockout (DKO) mice showed no abnormalities in cell localisation in the spleen or lymph nodes and no difference in antibody titres following thymus-dependent (TD) immunisation. However, IgM and IgG3 titres were increased in the thymus-independent 2 response. In the spleen, B cell numbers were increased at rest, but normal after TD immunisation; while in lymph nodes B cell numbers were decreased both before and after TD immunisation. Together, the minor difference in phenotype in these DKO mice compared to controls indicates separate roles of CCRL1 and CCRL2 in the antibody response. Additional studies into these receptors individually will lead to further elucidation of their functions.

List of abbreviations:

ACKR - Atypical chemokine receptor
APC – Antigen presenting cell
B220 – B cell isoform of 220 kDa
BCR – B cell receptor
CCL – CC chemokine ligand
CCR – CC chemokine receptor
CCRL1 – CC-Chemokine receptor-like 1
CCRL2 – CC-Chemokine receptor-like 2
CD – Cluster of differentiation
CGG – Chicken gamma globulin
CMKLR1 - Chemokine-like receptor-1
CXCL – CXC chemokine ligand
CXCR – CXC chemokine receptor
DC – Dendritic cell
DKO – Double knockout ($CCRL1^{-/-}CCRL2^{-/-}$)
DZ – Dark zone
EBI2 – Epstein-Barr virus-induced G-protein coupled receptor 2
EBI2L - Epstein-Barr virus-induced G-protein coupled receptor 2 ligand
FDC – Follicular Dendritic cell
GC – Germinal centre
GPCR – G-protein coupled receptor
Het – Heterozygous $CCRL1^{-/-}CCRL2^{-/-}$ mouse
HEV – High endothelial venule
ICOS – Inducible costimulator
Ig – Immunoglobulin
IL – Interleukin
iLN – Inguinal lymph node
LN – Lymph node
LPS – Lipopolysacharide
LZ – Light zone
MALT – Mucosal associated lymphoid tissue
MHC - Major Histocompatability Complex
mLN – Mesenteric lymph node
MZ - Marginal zone
NP – Nitrophenol
PALS – Periarteriolar sheat
pLN – Popliteal lymph node
PNA – Peanut agglutinin
S1P – Sphingosine-1-phosphate
S1PR2 – Sphingosine-1-phosphate receptor 2
SLO – Seconary lymphoid organ
TD – Thymus-dependent
T_{FH} – T follicular helper cell
TI – Thymus-indepdendent
TZ – T Zone
WT – Wild type

1. INTRODUCTION

1.1 – Secondary lymphoid organs & B cell activation

Adaptive immune responses begin in secondary lymphoid organs (SLOs), which include lymph nodes (LNs) and the spleen. The spleen is located in the abdomen, adjacent to the stomach and just below the diaphragm. Functionally and structurally it is comprised of two parts: the red pulp, important for filtering blood – removing aged erythrocytes, bacteria and cellular debris; and the white pulp, involved in adaptive immune responses and the generation of antibody[1]. The white pulp consists of a central arteriole surrounded by the periarteriolar sheath (PALS) or T cell zone (TZ) where T cells and dendritic cells (DCs) interact. Around the TZ are B cell follicles where germinal centres can form as part of an immune response. Surrounding this structure is the marginal zone (MZ) which contains marginal zone macrophages (including marginal zone metallophilic macrophages), marginal zone B cells and a subset of dendritic cells. Exterior to the MZ is the marginal sinus which separates the white pulp from red pulp areas and allows entry of immune cells to the white pulp[1].

Lymph nodes act as garrisons for the immune system, formed at specific sites to sample antigens from the nearby tissue and augment the response against invading pathogens. LNs are comprised of an outer cortex and an inner medulla. Lymph enters via the afferent lymphatic vessels and travels through the cortical sinuses, into the medullary sinuses, and exits via the efferent lymphatics. Immune cells can enter the lymph node via this route or via high endothelial venules (HEVs) from the blood[2]. Unlike lymph nodes, the spleen has no afferent lymph vessels - immune cells can only enter via the blood[1].

The structure of the LN, although different, has similarities to that of the splenic white pulp. For example, the cortex is comprised of B cell follicles and a deeper paracortical area or TZ[2]. Both areas display a similar cellular composition to those in the spleen. In the LN medulla, medullary sinuses are separated by medullary chords that contain plasma cells, memory T cells and macrophages[2].

After entering a secondary lymphoid organ, B cells sample both free antigen, and antigen held in complexes on follicular dendritic cells (FDCs) in the B cell follicles[3]. Upon interacting with cognate antigen, a B cell will become activated. The fate and subsequent response elicited by this B cell will then depend on the nature of the antigen, as discussed below.

1.1.1 –Thymus dependent activation

Following activation by a conventional protein antigen, B cells are induced to migrate towards the TZ. Recognition of the antigen displayed on the B cell surface by a T cell will then cause local growth of both cells. B cells can then differentiate via one of two main pathways: the extrafollicular pathway, or the germinal centre (GC) response[4]. The extrafollicular pathway enables the rapid production of moderate affinity antibody, while the GC response facilitates the selection of high affinity antibody over a longer time period. Together, the two pathways allow an extremely efficient response to form as pathogens are met quickly with an initial wave of antibody, followed by a later wave of antibody of even greater affinity.

In the extrafollicular response, B cells first upregulate the transcription factor Blimp1 and differentiate into plasmablasts. These cells migrate to extrafollicular locations (such as the red pulp in the spleen) and associate with $CD11c^{high}$ DCs. These cells have shown to be important in aiding B cell survival[4]. CD138 (syndecan-1), a marker

for plasma cells, is progressively upregulated and antibody secretion is increased as plasmablasts become fully differentiated plasma cells. Most of these plasma cells have an approximate lifespan of 3 days in mice[4].

Alternatively, GCs may form in the B cell follicles, and are comprised of two main areas - a light zone (LZ) and a dark zone (DZ) (**Fig. 1.1**). The DZ is proximal to the T cell area while the LZ forms distally. This positioning of the light zone facilitates the uptake of antigen by resident follicular dendritic cells (FDCs)[5]

The purpose of a GC is to provide a specific niche to allow optimum affinity maturation –the process whereby a B cell increases the affinity for target antigen in order to generate a more specific humoral response. The classic description of the GC response first describes the migration of B cells to the DZ, where they become centroblasts. Here they rapidly proliferate and rearrange their antibody variable region immunoglobulin genes in a process known as somatic hypermutation[5]. This allows the random generation of higher affinity BCRs by introducing specific point mutations. T cell interactions may also promote further Ig heavy chain rearrangements that alter the immunoglobulin class - class switch recombination. Following this, cells exit the cell cycle and migrate to the LZ to compete for antigen held in complexes on FDCs. Successful B cells take up the antigen, while the majority of the B cells die by neglect, undergoing apoptosis before they are cleared by resident tingible body macrophages. Selected B cells must then receive help from follicular helper T (T_{FH}) cells in order to complete the final checkpoint. This help has shown to be essential as T_{FH} cells provide ICOS and CD40L signals, without which GC development is severely impaired[6]. The successful B cell can then become

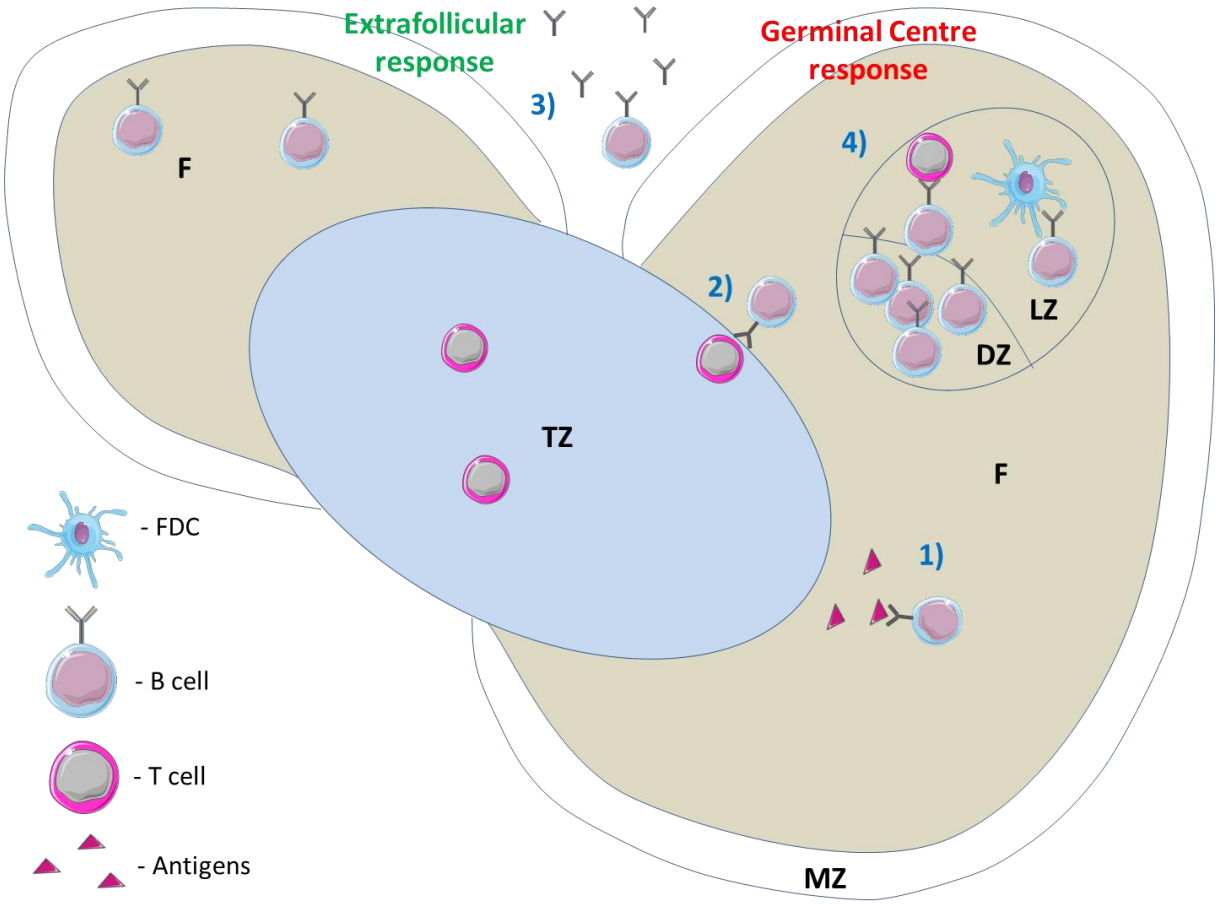

Figure 1.1 – Extrafollicular and germinal centre thymus dependent B cell responses in secondary lymphoid organs.

1) A B cell entering the secondary lymphoid organ encounters and internalizes cognate antigen and is activated. Antigen is processed and presented on MHC class II molecules. CCR7 is upregulated allowing movement towards the T cell zone. T cell activation in the T cell zone has also allowed upregulation of CXCR5 and subsequent migration towards the B cell follicle (not shown). **2)** Cognate B and T cells interact at the T zone border allowing bi-directional activation. B cells completing this step differentiate down one of two pathways. **3)** A B cell can exit the follicle and produce relatively low affinity unswitched IgM antibody, or **4)** The B cell can enter the germinal centre reaction. The cell will first enter the dark zone to become a centroblast, proliferating and undergoing somatic hypermutations, before it migrates to the light zone as a centrocyte to compete for antigen held on follicular dendritic cells. Successful B cells must interact with T follicular helper cells before either exiting the germinal centre as high affinity, class switched plasma/memory cells, or undergo repeated rounds of affinity maturation to further increase antibody affinity.

MHC; Major Histocompatability Complex, TZ; T cell zone, F; B cell follicle, MZ; Marginal Zone, DZ; Dark Zone, LZ; Light Zone, FDC; Follicular Dendritic Cell.

a plasma cell secreting high affinity antibody, or a memory B cell that allows a rapid response to secondary challenge[7]. Alternatively the B cell can migrate back to the dark zone and undergo repeated rounds of proliferation, somatic hypermutation and selection to increase antibody affinity further (see **Fig. 1.1**). It is worth pointing out that recent studies have indicated not all proliferation and somatic hypermutation happens in the DZ. Allen et al. showed cell division and apoptosis occurred in both the LZ and the DZ, highlighting the need for an updated model of the GC reaction[5].

1.1.2– Thymus independent activation

Alternatively, certain antigens can initiate the B cells response without the need of T cell help. These are known as thymus independent (TI) antigens, which can be subdivided into two types. TI-1 antigens include the bacterial molecule lipopolysaccharide (LPS), which activate Toll-like receptors on the surface of B cells as well as binding to the BCR. Conversely, TI-2 antigens, such as the polysaccharide Ficoll, provoke B cell responses by repeating epitopes cross-linking multiple BCRs. The predominant response against TI antigens is the extrafollicular pathway, and IgM^+ ('natural') memory B cells can be formed as part of this response[7]. GCs are able to form in some TI responses, but they are short lived, and break down after approximately 4 days in mice, presumably due to the lack of T_{FH} cell involvement. No plasma cells or memory B cells are thought to arise from these short lived GCs[4].

1.2– Chemokines and chemokine receptors in adaptive immune responses

1.2.1 – Conventional chemokine receptors

Chemokines (chemotactic cytokines) are small proteins that are involved in cellular trafficking and activation, as well as other diverse physiological functions including haematopoiesis, angiogenesis and central nervous system development[5, 8, 9].

Chemokine nomenclature is based on their structure. The main chemokines contain four cysteine residues that form disulphide bonds. Chemokines can be classified into groups depending on the amino acid composition at the position of the first and second cysteine residues in the sequence[10]. CC chemokines have no residues between these cysteines, whereas CXC- and CX3C chemokines have one or three residues respectively. Other chemokine groups lack 2 of the 4 cysteine residues – XCL1 and XCL2 chemokines[11]. Receptors for chemokines are G-protein coupled receptors (GPCRs). These are cell surface receptors that contain seven transmembrane regions and signal using intracellular G-protein subunits.

In adaptive immune responses, chemokines are vital for proper cellular positioning and colocalisation. Upon uptake of antigen, DCs upregulate CCR7 which allows them to enter SLOs as the CCR7 ligand CCL21 is expressed in the efferent lymphatic vessels. CCR7 is also important in allowing the migration of DCs to the TZ where stromal cells express the two CCR7 ligands CCL21 and CCL19 [12].

CCL19 and CCL21 are also involved in the retention of $CCR7^+$ T cells in the TZ. FDCs in the follicles express CXCL13 which is important in retaining $CXCR5^+$ B cells[12]. On recognition of antigen and subseqent activation, T cells downregulate CCR7 while upregulating CXCR5, allowing them to move towards the border of the B cell follicles. Conversely, once activated by antigen, B cells upregulate CCR7, allowing them to move towards the TZ and get help from activated T cells[12].

Once activated at the T cell border, B cells upregulate Epstein-Barr virus-induced G-protein coupled receptor 2 (EBI2), allowing their coordinated migration towards the outer edge of the follicle due to the high abundance of its ligand, EBI2L, in these areas[13]. By day 4 post antigen encounter, GC precursor B cells decrease expression

of EBI2 and upregulate sphingosine-1-phosphate receptor 2 (S1PR2) which directs migration to the centre of the germinal centre. Upon ligation of sphingosine-1-phosphate (S1P), S1PR2 inhibits chemokine-directed migration. The highest S1P concentrations are thought to be at the GC border, therefore S1PR2 B cells act to confine the GC BCs in the GC[13].

GC DZ B cells express high levels of CXCR4, which is necessary for cellular retention in the DZ in response to the ligand CXCL12. CXCL12 is thought to be produced by stromal cells that are more closely packed in the DZ. Conversely, CXCR5 expression is uniform across the GC, and as such downregulation of CXCR4 allows the GC B cells to respond to CXCL13 signals and move into the light zone to compete for antigen[5]. Interestingly, in the MZ, the atypical chemokine receptor CXCR7 was shown to be expressed on MZ B cells acting as a chemokine sink, taking up and degrading CXCL12[14].

1.2.2 – Atypical chemokine receptors – CCRL1 and CCRL2

Atypical chemokine receptors (ACKRs) differ from their conventional chemokine receptor counterparts by their inability to the initiate classical GPCR signalling response[15, 16]. The canonical motif DRYLAIV in the second intracellular loop is either absent or altered in ACKRs. This abolishes the ability of the receptor to couple to G-proteins. There are currently five known ACKRs: Duffy Antigen Receptor for Chemokines (DARC), D6, CXCR7 and CC-Chemokine receptor like 1 and -2 (CCRL1 and CCRL2)[16]. ACKRs share the propensity to internalize chemokines. This uptake is followed by either degradation or transport of the chemokine depending on the ACKR[15].

CCRL1 has been shown to be expressed in lymphatic endothelial cells and cortical thymic epithelial cells[15, 17-19]. Initially, it was thought CCRL1 was not expressed on hematopoietic cells[17], but data from the Immunological genome project and our lab show CCRL1 mRNA is present in GC B cells. Our lab has since confirmed this at the protein level by immunofluorescence staining [Laura Ibanez - unpublished data].

CCRL1 binds the CCR7 ligands CCL19 and CCL21; the CCR9 ligand CCL25 and in humans can bind the CXCR5 ligand CXCL13 with low affinity[15, 20, 21]. Upon ligand binding, CCRL1 recruits β-arrestin and is transported, along with the bound chemokine, to lysosomes for degradation[15, 16]. CCRL1-deficient mice show increased blood titres of CCL21 as well as increased titres of both CCL21 and CCL19 in lymph nodes. Intriguingly, this was coupled with a decreased LN cellularity and reduced DC influx to LNs following immune challenge[16, 22]. This could be as a failure of CCRL1$^{-/-}$ mice to establish pro-migratory chemokine patterns or due to CCR7 desensitisation[16].

CCRL1 may be involved in controlling the gradients of CCL19 and CCL21 in the tissue to aid entry of CCR7-expressing immune cells into SLOs[15]. Similar mechanisms may operate in the thymus. Aged CCRL1-deficient mice develop autoimmunity, potentially due to abnormal thymocyte migration patterns and failures in central tolerance[15]. Therefore, it could conceivably be the case that CCRL1-mediated scavenging of CCR7 ligands may help keep CCR7^{hi} T cells out of the GC, and permit memory and plasma cells to leave following affinity maturation and selection.

CCRL2 is the most recently discovered member of the ACKR family, and as such it has been least characterised. Reports suggest it binds to CCL5 and CCL2, but these

findings have not yet been independently confirmed, leading some to question its status as a true chemokine receptor[16, 23]. However, CCRL2 has been shown to bind the adipokine chemerin, and in humans it binds and internalizes CCL19[16, 24, 25]. CCRL2 has been shown to be expressed on almost all haemopoetic cells, including B cells, T cells, DCs and macrophages[16, 26].Within B cell subsets, data from our lab have shown CCRL2 expression is highest in plasma cells [Sarah Cook - unpublished data].

One study demonstrated DCs from CCRL2-deficient mice are defective at transporting antigen to mediastinal lymph nodes in a model of airway inflammation[27]. Another study revealed CCRL2 transfected cells are able to concentrate chemerin at inflammatory sites, allowing its presentation to another chemerin receptor Chemokine-like receptor 1 (CMKLR1)[24, 26]. Building from this, CCRL2 has also been shown to play a role in lymphocyte recruitment. The CCRL2 expressed on endothelial cells concentrated chemerin to the inflammatory site where it mediated the recruitment of $CMKLR1^{+}$ lymphocytes[28]. Relating to the B cell response, data from our lab has shown CCRL2-deficient mice display increased serum IgM titres, and splenic plasma cell numbers in response to the TI-2 antigen NP-Ficoll [Sarah Cook - unpublished data].

1.3 – Study aims

The little known roles of both CCRL1 and CCRL2 make both these receptors interesting options for study. Furthermore, the two receptors are located on the same chromosome, and are relatively close proximity – approximately 6MB apart. Therefore, in evolutionary terms, it is plausible that these genes arose by recent gene duplication and thus may have overlapping functions. For that reason the aims of this project were to investigate any differences in antibody responses in mice deficient in

both these receptors. Both thymus-dependent and –independent 2 responses were comprehensively analysed. In collaboration with two ongoing PhD projects looking at the roles of CCRL1 and CCRL2 individually, this work could have important implications in unravelling the function and significance of these receptors in B cell responses.

2. MATERIALS AND METHODS

2.1 – Mice

All mice were housed at the University of Birmingham biomedical services unit (BMSU) and treated according to Home Office guidelines. Wild type (WT) C57 BL/6 mice were purchased from Harlan Laboratories. CCRL2 deficient mice ($CCRL2^{-/-}$) were purchased from The Jackson Laboratory, ME, USA. CCRL1 deficient mice ($CCRL1^{-/-}$) were a kind gift from R.Nibbs [University of Glasgow]. These two deficient strains were then crossed. Crossovers of both genes were identified by producing F1 hybrid mice, and then by crossing F1 hybrids onto wildtype mice. F2 offspring was screened for the presence of both alleles. Presence of a copy of each allele in F2 mice identified crossovers. These mice were then inbred to produce double deficient CCRL1/CCRL2 mice. Heterozygous CCRL1/CCRL2 deficient mice were also produced from backcrosses onto the C57 BL/6 strain.

2.2 – Immunisations

Immunisations were carried out using both the thymus dependent antigen nitrophenol-chicken gamma globulin (NP-CGG) and the thymus independent type II antigen 4-hydroxy-nitrophenyl-Ficoll (NP-Ficoll). CGG [Sigma] was conjugated to NP by Mrs. Chandra Raykundalia [school of Immunity and Infection, University of Birmingham]. 9% aluminium potassium sulphate was mixed with NP-CGG and the

pH adjusted to 6.5 to create an alum precipitate. The suspension was mixed in the dark before centrifugation (5 mins, 2000rpm). NP-CGG was then washed twice in PBS and resuspended in saline at a concentration of 50µg/200µl with 1 x 10^7 heat killed *Bordetella* p*ertussis*/ml for intraperitoneal (i.p.) injections; or at a concentration of 20µg/20µl with 5 x 10^6 heat killed *Bordetella* p*ertussis pertussis/*ml for footpad injections. *Bordetella pertussis* was added as a further adjuvant. NP-Ficoll [Biosearch Technologies, Novato, CA] was prepared by dissolving the antigen in PBS at a concentration of 30µg/200µl.

2.3 – Isolation of spleen, lymph node and serum

Blood was extracted by cardiac puncture and incubated briefly at 37°C to allow for clotting, before centrifugation (10000rpm, 10 minutes). Supernatant was removed and stored at -20°C. Spleens and lymph nodes were isolated by dissection and weighed. The central portions of the spleens or whole LN were snap frozen in liquid nitrogen or dry ice. The ends of the spleens, along with some LNs, were mashed into RPMI 1640 media [Sigma-Aldrich] containing 10% heat inactivated fetal calf serum (FCS) and the antibiotics penicillin/streptomycin (RPMI +FCS+P/S). Cells were then counted with a haemocytometer, using a 1/10 dilution of trypan blue. Cells were centrifuged and resuspended at the appropriate concentration(s).

2.4 –Flow cytometry

Cell suspensions were transferred to a 96 well plate. A 1:1 ratio of control and knockout (CCRL1/CCRL2$^{-/-}$) cells were also used for compensations and unstained controls. The plate was first centrifuged (4 mins, 1000rpm, 4°C), and the cells resuspended with 50µl of anti-FcRγII and –FcRγIII antibodies (to prevent non-specific binding) in FACS buffer [Sigma-Aldrich] containing 10% FCS and 2mM EDTA. Cells were incubated with this block for 20 minutes at 4°C. Following this, 150µl of wash

buffer (RPMI +FCS+P/S) was added to each well, the plate centrifuged (4 mins, 1000rpm, 4°C) and incubated in 50µl of relevant antibody mixes (20mins at 4°C). This incubation step was carried out in the dark to prevent unnecessary photobleaching. Cells were then washed twice before being transferred in FACS buffer to FACS tubes for running on the flow cytometer. In the case of biotinylated antibodies, incubation periods were 1 hour, and then a wash step was carried out before streptavidin conjugated to PE Cy-7 was added for 20 minutes. Analysis was carried out on a CyAN flow cytometer [Beckman Coulter, UK] using Summit v4.3 software. FloJo v9.3.2 software was used for subsequent offline analysis. All antibodies and dilutions used are listed in table 1.

2.5 – Immunohistochemistry

Sections of spleen and LN were cut using a cryostat to a thickness of 6µm, and transferred to glass slides. Slides were fixed in acetone (20 mins, 4°C) and stored at -20°C until required. For staining, slides were first washed in Tris buffer (pH 7.6) for 10 minutes and then incubated with primary antibodies (made up in Tris buffer) for 1 hour at room temperature in a humidity chamber. Slides were then washed in Tris buffer for 5 minutes and then secondary antibodies added in Tris buffer with 10% normal mouse serum (NMS) [Dako, Ely, UK] to minimise non-specific binding to the sections. After a 45 minute incubation period, slides were washed in Tris buffer as before. Next, streptavidin complex [Dako] was added to the slides to bind to biotinylated secondary antibodies for 45 minutes. After washing, slides were stained with horseradish peroxidase substrate 3,3 diaminobenzidine tetrachloride (DAB) [Sigma] and visualised after approximately 5 minutes. When slides were adjudged to have been sufficiently developed, they were washed and then incubated with the substrate for alkaline phosphatase, Fast Blue [Sigma]. Slides were visualised to

monitor development and then washed once more. Finally, slides were washed in distilled water and mounted using warm glycerol gelatine [Sigma]. Images were taken with a Leica CTR6000 microscope using a micropublisher 5.0RTV camera using Q Capture software v.2.9.11. Analysis was carried out using ImageJ v.1.46r software. All antibodies used are listed in table 1.

2.6 – Immunofluorescence histology

Slides were first blocked for 1 hour with 10% normal horse serum in PBS containing 1% bovine serum albumin (BSA). Relevant primary, secondary and tertiary antibodies were then added sequentially. Primary antibodies were incubated for 1 hour, while secondary and tertiary antibodies were incubated for 45 minutes each. All incubation steps were carried out in a dark humidity chamber with 5 minute washing steps in phosphate buffered saline (PBS) between each stain. All antibodies were made up in PBS – 1% BSA, and secondary antibody solutions also contained 10% NMS to prevent non-specific binding. After a final wash step, slides were mounted using prolong gold (Life Technologies) and stored in the dark until use. Images were taken with the same Leica microscope (see section 2.5), but using LAS AF v.2.6.0.7266 software. Analysis was carried out using ImageJ v.1.46r software. All antibodies used are listed in table 1.

2.7 – ELISA

96 well ELISA plates [Immuno 96 MicroWell solid – Nunc, Thermo Scientific] were coated with 5µg/ml NP_2-BSA or NP_{15}-BSA in coating buffer (Na_2CO_3 15mM, $NaHCO_3$ 35mM) overnight at 4°C. NP_2-BSA was used to detect high affinity antibody, while NP_{15}-BSA was used to detect total antibody. Conjugation of both antigens was carried out by Mrs. Chandra Raykundalia [school of Immunity and Infection, University of Birmingham]. After incubation, plates were washed in wash buffer (PBS

100nM, 0.05% Tween 20, pH 6.8) and blocked to reduce non-specific binding by adding 200µl of PBS containing 1% BSA to each well. Plates were incubated for 90 minutes in a humidity chamber at 37°C. Meanwhile, serum was diluted in PBS as required. After washing, serum was serially diluted across the plate to provide a range of concentrations to test, allowing for the post-experimental generation of standard curves.

Following another wash step, alkaline phosphatase-conjugated isotype specific antibody solutions were added to relevant wells and incubated for 1hr at 37°C. After subsequent washing, 100µl of the substrate p-nitrophenyl phosphate (N2770 – Sigma-Aldrich) was added to each well and the plate was incubated at 37°C until a yellow colour appeared. The plates were read at 405nm using a Synergy HT Microplate Reader [Bio-Tek, VT, USA] and SoftMax Pro v.5.4.5 software. Standard curves were produced and extrapolated on Microsoft Excel 2010. Results were first plotted as dilution against absorbance readings, before a manual threshold y-value was assigned at a point of logarithmic decline on the curves (**Fig. 2.1**). An x-value of dilution was then extrapolated from this threshold to give relative titres.

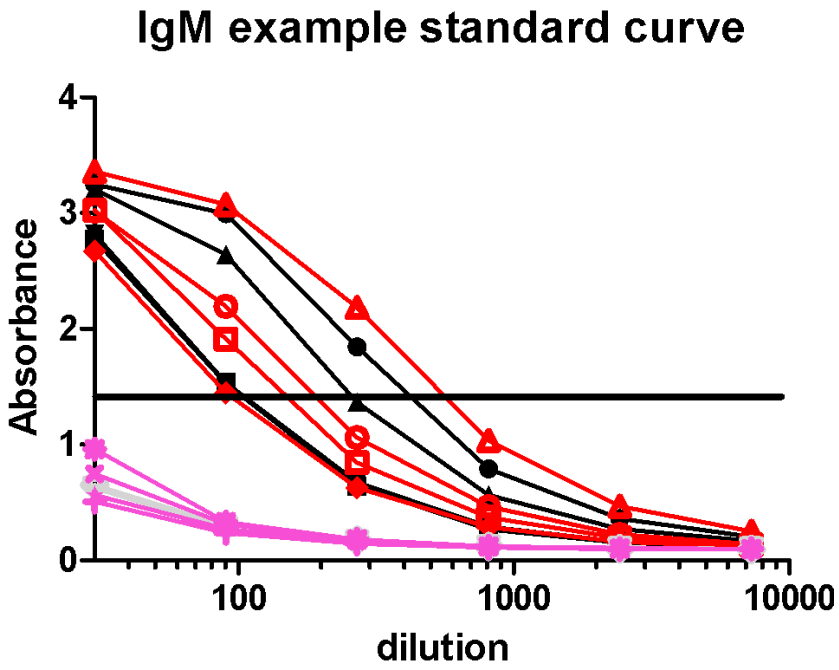

Figure 2.1 – Example standard curve to illustrate ELISA analysis. Black horizontal line indicates threshold taken to extrapolate dilutions and calculate relative antibody titres.

2.8 – Statistical Analysis

Data was plotted, analysed and displayed using GraphPad Prism v.5 software. Statistical significance was assessed by the non-parametric Mann Whitney U two-tailed test. P values of <0.05 were accepted as statistically significant.

2.9 – Antibody list

Specificity	Conjugation	Species/Isotype	Final Dilution	Experiment	Company (Reference no.)
Mouse IgD	-	Sheep	1/500	Immunohistochemistry	ABCAM (AB9177)
Mouse IgD	-	Rat	1/1000	Immunohistochemistry	BD Pharmingen (553438)
Mouse IgM	-	Rat	1/600	Immunohistochemistry	ABD serotec (MCA199)
Mouse IgG	-	Rat	1/100	Immunohistochemistry	ABD serotec (MCA424)
Mouse CD3	-	Rat	1/500	Immunohistochemistry	ABD serotec (MCA500G)
Mouse CD138	-	Rat	1/100	Immunohistochemistry	BD Pharmingen (553712)
NP	-	Sheep	1/3000	Immunohistochemistry	In House
Mouse F4/80	-	Rat	1/500	Immunohistochemistry	ABD serotec (MCA497GA)
Rat Igs	Biotin	Rabbit	1/600	Immunohistochemistry	DAKO (E0468)

Specificity	Conjugation	Species/Isotype	Final Dilution	Experiment	Company (Reference no.)
Sheep Igs	Peroxidase	Donkey	1/100	Immunohistochemistry	Jackson Immunoresearch (713-035-147-JIR)
Sheep Igs	Biotin	Donkey	1/100	Immunohistochemistry	Jackson Immunoresearch (713-065-147-JIR)
Rat Igs	Peroxidase	Rabbit	1/80	Immunohistochemistry	DAKO (P0450)
Mouse CD16/CD32	-	Rat IgG2b, k	1/200	Flow cytometry	BD Pharmingen (01241A)
Mouse IgD	FITC	Rat IgG2a, k	1/300	Flow cytometry	BD Pharmingen (553439)
Mouse IgM	PE-Cy7	Rat IgG2a, k	1/500	Flow cytometry	eBioscience (25-5790-82)
Mouse B220	eFlour450	Rat IgG2a, k	1/50	Flow cytometry	eBioscience (558108)
Mouse B220	PE-Texas Red	Rat IgG2a, k	1/500	Flow cytometry	BD Pharmingen (551489)
Mouse B220	FITC	Rat IgG2a, k	1/100	Flow cytometry	BD Pharmingen (553088)
Mouse CD3	PerCP-Cy5.5	Hamster IgG1, k	1/200	Flow cytometry	BD Pharmingen (551163)
Mouse CD3	PE	Hamster IgG1, k	1/200	Flow cytometry	BD Pharmingen (553064)
Mouse CD4	APC	Rat IgG2a, k	1/300	Flow cytometry	eBioscience (17-0042-82)
Mouse CD4	PE	Rat IgG2b, k	1/500	Flow cytometry	BioLegend (116006)
Mouse CD4	PerCP Cy5.5	Rat IgG2a, k	1/300	Flow cytometry	BD PharMingen (550954)
Mouse CD11b	PE	Rat IgG2b, k	1/1000	Flow cytometry	eBioscience (12-0112-83)
Mouse CD11c	APC	Rat IgG2b, k	1/500	Flow cytometry	eBioscience (17-0114-82)
Mouse CD19	APC	Rat IgG2a k	1/200	Flow cytometry	BD PharMingen (550992)
Mouse CD21/CD35	APC	Rat IgG2b, k	1/100	Flow cytometry	BD Pharmingen (558658)
Mouse CD23	PE	Rat IgG2a, k	1/200	Flow cytometry	BD Pharmingen (553139)
Mouse CD38	Pacific Blue	Rat IgG2a, k	1/400	Flow cytometry	BD Pharmingen
Mouse CD38	Alexa Fluor 700	Rat IgG2a, k	1/400	Flow cytometry	eBioscience (56-0381-82)
Mouse CD86	PE-Cy5	-	1/200	Flow cytometry	eBioscience
Mouse Fas (CD95)	PE-Cy7	Hamster IgG	1/150	Flow cytometry	BD Pharmingen (557653)
Mouse CD138	APC	Rat IgG2a, k	1/100	Flow cytometry	BD Pharmingen (558626)
Mouse PD-1 (CD279)	PE	Rat IgG2b, k	1/100	Flow cytometry	BD Pharmingen (551892)
Mouse CXCR4 (CD184)	FITC	Rat IgG2b	1/100	Flow cytometry	BD Pharmingen (551967)
Mouse CXCR5	Biotin	Rat IgG2a, k	1/50	Flow cytometry	BD Pharmingen (551960)

Specificity	Conjugation	Species/Isotype	Final Dilution	Experiment	Company (Reference no.)
Isotype control	-	Rat IgG2a, k	1/50	Flow cytometry	-
NP*	PE	-	1/2000	Flow cytometry	
Mouse IgD	FITC	Rat IgG2a, k	1/100	Immunofluorescence	BD Pharmingen (553439)
Mouse IgD	APC	Rat IgG2a, k	1/100	Immunofluorescence	eBioscience 17-5993-80
Mouse CD73	-	Rat IgG1	-	Immunofluorescence	eBioscience (14-0731-81)
Mouse CD80	-	Hamster IgG1 k	1/100	Immunofluorescence	BD PharMingen (09601D)
Mouse CD138	-	Rat IgG2a, k	1/200	Immunofluorescence	BD PharMingen (553712)
Mouse CD169	-	Rat	1/100	Immunofluorescence	AbD Serotech MCA947
Mouse CXCR4 (CD184)	-	Rat IgG2b	1/100	Immunofluorescence	BD PharMingen (551852)
Mouse Ki67	-	Rabbit	1/400	Immunofluorescence	Gift from J. Gerdes, Research Centre Borstel, Germany
Rat Igs	FITC	Donkey	1/100	Immunofluorescence	Jackson Immunoresearch (712-096-153)
Rabbit Igs	Cy3	Donkey	1/100	Immunofluorescence	Jackson Immunoresearch (711-165-152)
Hamster Ig	Biotin	Goat	1/100	Immunofluorescence	Vector R0707
FITC	Alexafluor 488	Goat	1/100	Immunofluorescence	Invitrogen (A11096)
FITC	Alexafluor 488	Rabbit	1/100	Immunofluorescence	Invitrogen (A11090)
Mouse IgM	Alkaline Phosphatase		1/2000	ELISA	AbD Serotech
Mouse IgG	Alkaline Phosphatase		1/1000	ELISA	AbD Serotech
Mouse IgG1	Alkaline Phosphatase		1/1000	ELISA	AbD Serotech
Mouse IgG3	Alkaline Phosphatase		1/1000	ELISA	Southern Biotech

Table 2.1 - List of antibodies used in this study (*NP is not itself an antibody, but is included for completeness). APC - Allophycocyanin , PE - Phycoerythrin, Cy3 – Cyanine 3. Cy5 – Cyanine 5, Cy7 - Cyanine 7, PerCP - Perdinin-chlorophyll protein, FITC - Fluorescein isothiocyanate.

3. RESULTS

3.1 – Unimmunised DKO mice display increased T and B cell numbers in the spleen, but splenic architecture and cellular composition is largely unaffected in thymus-dependent responses

First, we wanted to compare spleen sections of CCRL1/2 double knockout (DKO) mice with wild-type (WT) mice to look for any obvious histological defects. The T cell areas and B cell follicles were present and looked structurally similar in both mice, as shown by CD3 and IgD staining respectively (**Fig. 3.1A**). $IgM^{+}IgD^{-}$ Marginal zone B cells were present in the marginal zones of the white pulp areas, and $CD138^{+}$ plasma cells were also evident in the red pulp areas in both DKOs and WT controls. Both cell types appeared present in similar numbers. Mature red pulp macrophages express the surface molecule F4/80. The sections clearly show the presence of these macrophages in the DKO mice at a high density and clearly confined to the red pulp, similar to controls. Together these results suggest there is no clear defect in splenic microarchitecture, or deficiency in naive B cells, plasma cells, extrafollicular B cells, T cells or red pulp macrophages in the spleens of DKO mice.

We next sought to examine the architecture of the spleen in the TD response of DKO mice. Mice were immunized with NP-CGG both i.p. and in the footpad and the response analysed at day 8. As expected, TZ and follicular structure was unaltered at this time point (**Fig. 3.1B**). The response to NP was evident in some mice from both the DKO and heterozygous (het) control groups. The reason some mice had not produced a response to NP by day 8 are unclear, but this is most likely due to problems with immunisations. Of those that responded, NP staining is denser in the LZ of germinal centres as this is where most FDCs hold immune complexes of antigen and specific antibodies that bind NP. Strong NP staining is also evident in

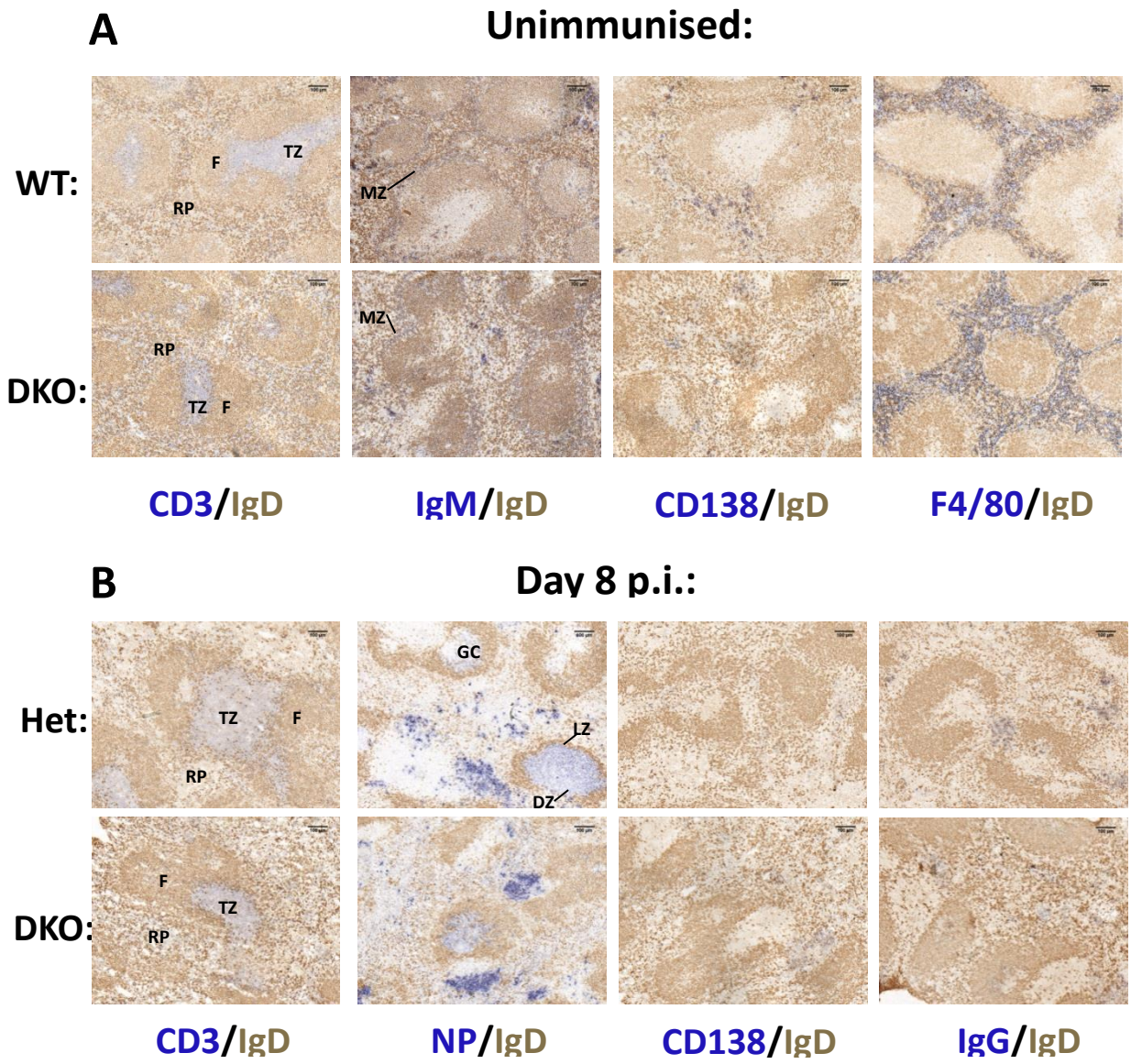

Figure 3.1 - Comparison of splenic architecture in DKO mice and controls.

A – Immunohistochemistry staining on sections from unimmunised DKO mice (n=4) and WT controls (n=2). Sections were stained for CD3, IgM, CD138 and F4/80 (blue) and IgD (brown). **B -** Immunohistochemistry staining on sections from mice day 8 post immunization (p.i) with the TD antigen NP-CGG. Staining was for CD3, NP, CD138 and IgG (blue) and IgD (brown). Heterozygous (Het) mice were used as controls (n=4) along with test DKO mice (n=2)

Representative images are shown. Scale bars represent100μm in length. TZ – T cell zone; F – B cell follicle; RP – red pulp; MZ – marginal zone; GC – germinal centre; DZ – dark zone; LZ – light zone.

some red pulp areas, representing NP^+ plasma cells. Furthermore, a few NP^+IgD^- cells can be seen around the GC, but still in the B cell follicle, most likely representing newly generated memory B cells. There were no noticeable differences in any localisation or density of any of these cell types in DKOs compared to controls.

Plasma cells were present in both groups at day 8 p.i., although overall there may have been slightly more plasma cells in the DKO. However, as numbers of mice with successful immunisation leading to plasma cell generation were too low (n=2 for DKO), these results have not been deemed significant. Lastly, IgG was seen in similar amounts in the red pulp areas of DKO and het mice, indicating that class switching to IgG was present in the absence of CCRL1 and CCRL2. Overall, results indicate architecture and key cell types are very similar between DKO and control mice.

When looking at the spleen sections as a whole it was noticed that some of the germinal centres in the DKO mice looked 'rugged' – i.e their edges were not clearly defined and merged into IgD^+ areas of the B cell follicle (Fig. 3.1B). This would agree with the hypothesis discussed above that CCRL1 has a role in cellular positioning within the GC. Therefore, a blinded test was carried out where GCs were classed as rugged or non-rugged. However, the data obtained from these blinded counts do not show a relationship between irregular GCs and CCRL1/2 deficiency (**Fig. 3.2**). To give conclusive results this experiment should be repeated on a larger group of samples. Further, the development of a more objective method to measure whether a GC is rugged than the subjective microscopic decision used here would be helpful.

Alongside the histological analysis, flow cytometry was performed to look at any differences in cellular composition in the spleens of unimmunised DKO mice. The staining panel and gating strategy used allowed us to look at follicular and MZ B

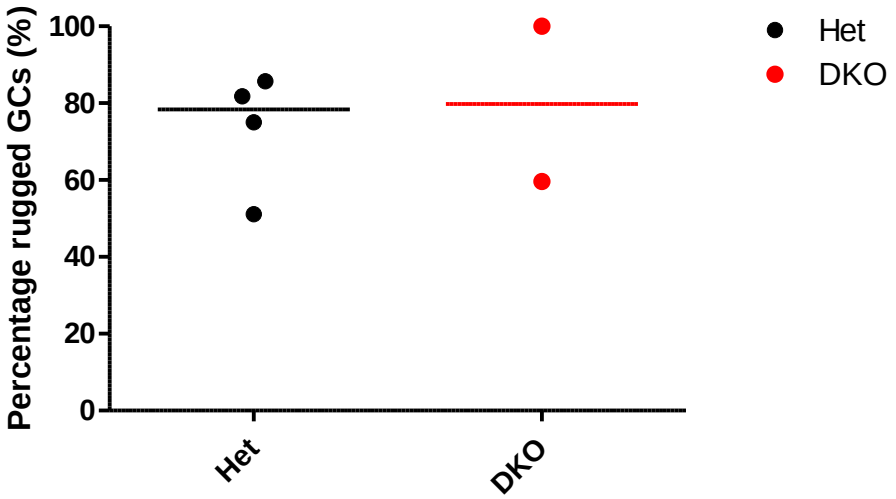

Figure 3.2 – Preliminary examination of GC 'ruggedness' in DKO and control mice d8 p.i.

Graph shows the median percentage of germinal centres deemed rugged in DKO and het controls day 8 p.i. Data was collected blinded to the origin of the mice to remove bias (het n=4, DKO n=2).

cells, and the T cell population (**Fig. 3.3A**). MZ B cells express high levels of CD21 and CD35 and low levels of CD21, as opposed to follicular B cells which express higher CD21 and IgD[29].

Results show a very slight increase in the percentage of overall B cells compared to controls, and a modest increase in T cell percentages (**Figs. 3.3B, C**). This is interesting as increased percentages of both B and T cells within the lymphocyte fraction would indicate other cell types (such as plasma cells or dendritic cells) were decreased correspondingly in DKO mice. Indeed, the ungated population within the lymphocyte gate represented a substantially smaller proportion of lymphocytes in DKO mice (data not shown). In absolute numbers, the increase in B cells and T cells is even more robust (**Fig. 3.3D**). Within the B cell subset, follicular B cells were increased in percentage and number in DKO mice, whereas MZ B cells showed minimal change. Thus, it appears DKO mice have an increased representation of B and T cells in the spleen.

Spleens from mice immunised with NP-CGG were also analysed by flow cytometry. Before maceration and staining, spleens were weighed. Interestingly, DKO spleens weighed slightly less on average than control spleens (**Fig. 3.4A**). B cells that responded to NP were gated on first, and a combination of anti-CD38, anti-Fas, anti-CD86 and anti-CXCR4 antibodies allowed us to identify GC B cell populations. An anti-CD138 antibody was used to identify plasma cells (for gating strategy see **figure 3.4B**)[30]. It is worth noting that CD38 staining was unsuccessful in this instance, so GC B cells were selected on Fas expression alone. Although memory B cells will also be included in this gate, the majority will still be GC B cells.

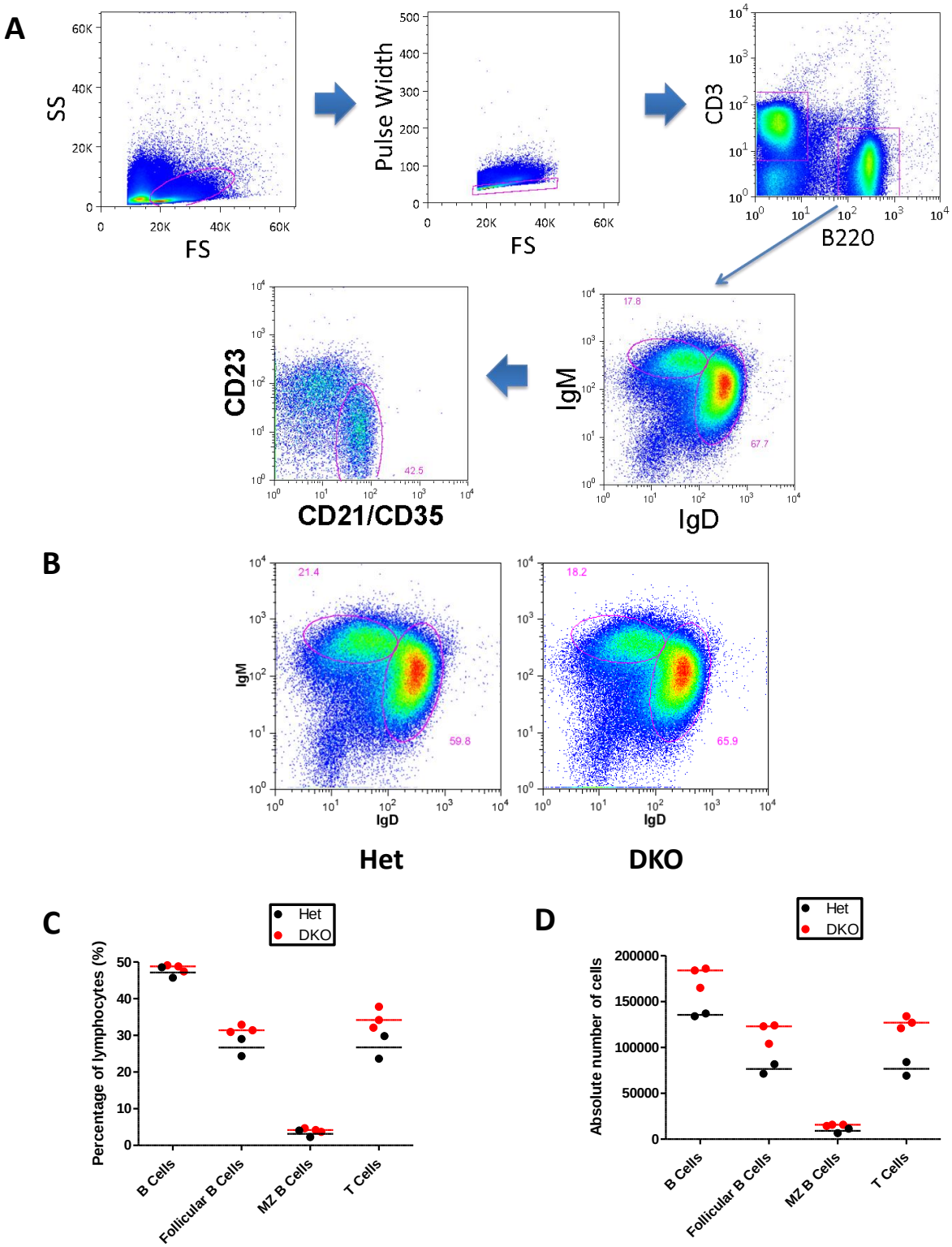

Figure 3.3 – Analysis of key splenic cell types in unimmunised DKO mice.

A – Gating strategy used. Live lymphocytes were first gated on according to their forward and side scatter properties. Singlet lymphocytes were then gated on before gates were set on $CD3^{high}B220^{low}$ cells (T cells) and $B220^{hi}CD3^{lo}$ cells (B cells). Within the B cell gate, IgD^{hi} cells were considered follicular B cells while $CD21/CD35^{hi}$ $CD23^{lo}$ cells within the IgM^{hi} gate were considered marginal zone B cells. Arrows indicate direction of gating. **B –** Representative IgD vs IgM plots from DKO and Het control. **C –** Comparison of key cell types in DKO (red circles) and Het mice (black circles). Data represented as percentage of singlet lymphocytes (**C**) and absolute cell number **(D).** Lines represent median values. Sample sizes: DKO = 3, Het = 2.

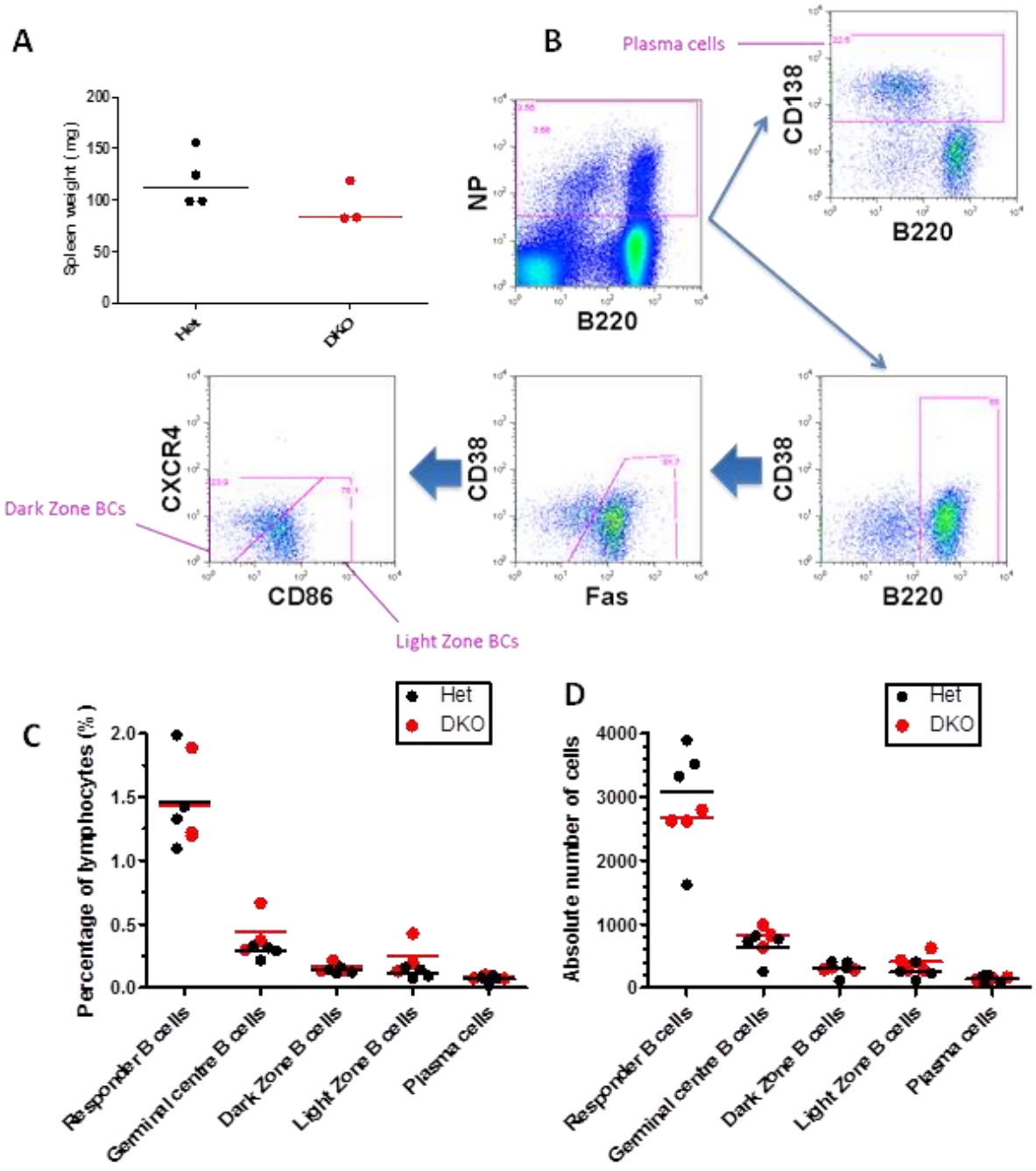

Figure 3.4 – Flow cytometric analysis of key cellular populations in the TD B cell response in the spleen day 8 p.i.

A – Comparison of spleen weights between DKO and Het. **B –** Gating strategy used. Live lymphocytes gated on (not shown), then NP^{+} responder cells. From here $CD138^{+}$ plasma cells , and $B220^{+}$ total responder B cell percentages were analysed (far right gates). $Fas^{hi}CD38^{lo}$ cells were gated on as total GC B cells, and finally CXCR4 and CD86 were used to distinguish DZ and LZ B cells (note gating strategy is identical to that used for lymph node [figure 3.8] and example shown is from lymph node sample in order to show a clear GC B cell population). Arrows represent gating direction. **C –** Percentage of singlet lymphocytes (**C**) and absolute number of cell (**D**) comparison between DKO and het mice. Lines represent medians, red – DKO, black – het. Sample sizes: DKO = 3, Het = 4.

Despite a reduced median weight of the DKO spleens, the numbers of B cells that responded to NP-CGG were unaffected in DKO mice (**Fig 3.4D**). Similarly, GC B cells and plasma cell numbers were unaltered. There were also no apparent differences in these subsets as a percentage of lymphocytes, although there was a slight trend of increased GC B cell and LZ B cell percentages in the DKO mice (**Fig. 3.4C**). This could suggest that DKO mice produce more GC B cells in a TD response by day 8 than het controls, although histology shows no obvious difference in germinal centre sizes or IgG class switching (**Fig. 3.1A**). However, more data is needed for a convincing conclusion to be drawn.

To test whether CCRL1 has a role controlling cellular trafficking of T cells in the GC, we also carried out a stain for T_{FH} cells – involved in selection of centrocytes in the LZ (see section 1.2.1). The CXCR5 antibody was biotinylated, requiring a second step addition of streptavidin conjugated toPE-Cy7. To control for this staining, both biotinylated isotype control antibodies, and streptavidin PE-Cy7 alone were used. Unfortunately minimal expression of CXCR5 was observed above background (**Fig. 3.5B**) indicating the staining procedure had failed. An analysis of $CD4^+$ cells showed no difference between DKO and het mice (**Fig. 3.5A, C**). This backs up the histology results seen previously where T cell numbers appear similar in both groups.

Overall, no apparent differences were seen in the splenic organization of DKO mice, both immunised and un-immunised. However, in terms of cellular composition, modest increases in B and T cells can be seen in the unimmunised DKO mice. At day 8 p.i. with NP-CGG, spleens of DKO mice appear slightly reduced in mass compared to controls (despite no B or T cell deficiency), and it is possible there are small increases in GC B cell percentages compared to controls. This could indicate a

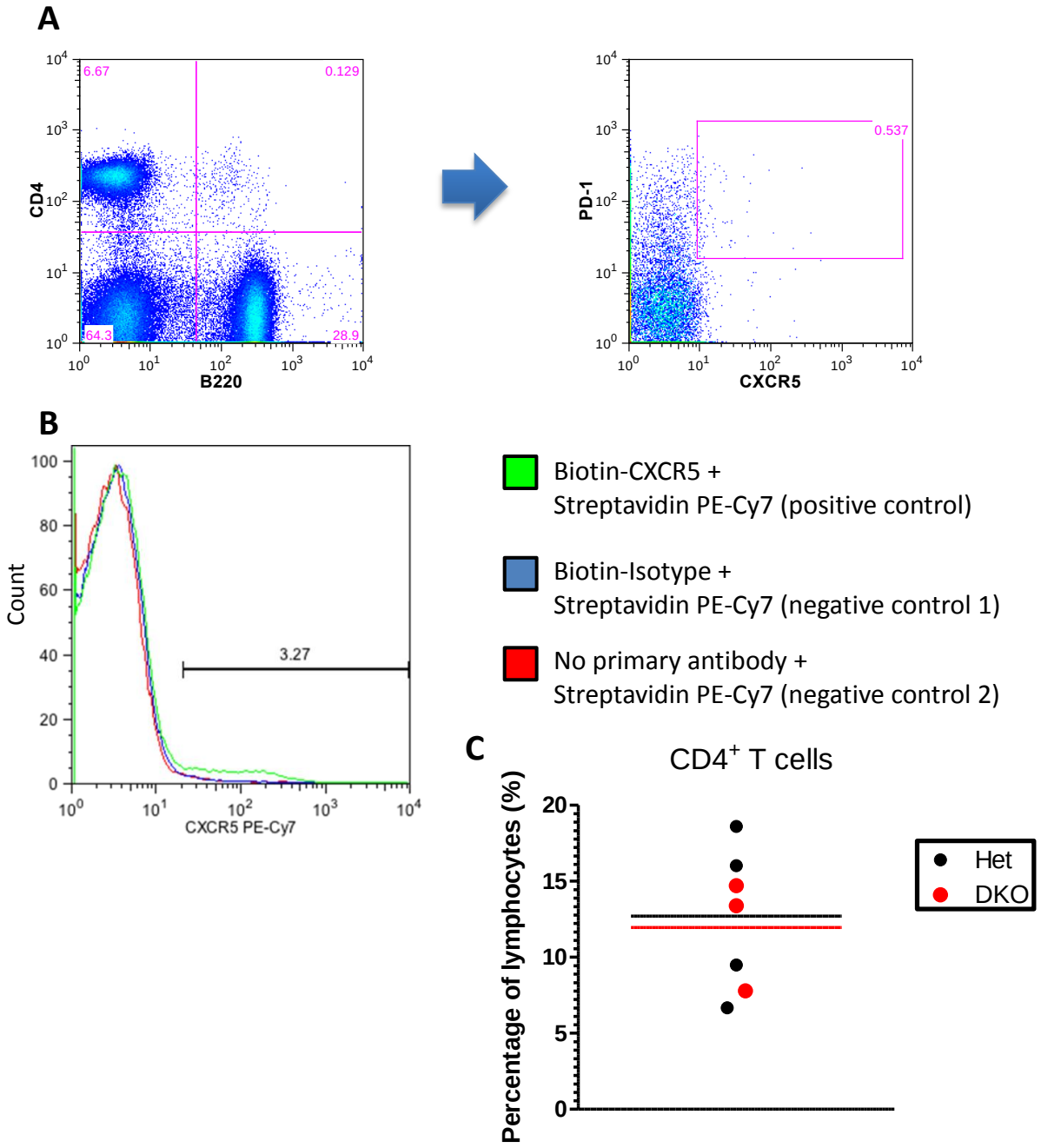

Figure 3.5 – T follicular helper stain on splenocytes day 8 p.i.

A – Gating strategy. Singlet lymphocytes were gated on (not shown) followed by $CD4^+$ cells and in this gate $PD\text{-}1^+CXCR5^+$ cells represented T_{FH} cells. **B –** Controls for CXCR5 PE-Cy7 stain. Frequency histograms show signal intensity in the PE-Cy7 channel: Green – biotinylated CXCR5 antibody, blue – biotinylated isotype control antibody and red no primary antibody. All samples had the anti-streptavidin PE-Cy7 antibody added after an incubation period. **C –** Comparison of $CD4^+$ T cells in DKO and het spleens as a percentage of lymphocytes.

slightly faster induction of the GC response, but results must be interpreted with caution due to small sample sizes and only modest differences in magnitude.

3.2 – Lymph node microarchitecture and cellular composition is unaltered in DKO LNs, but lymphocyte cellularity is reduced in the TD response and at rest

The next logical step was to look for any differences in lymph node populations. Overall B and T cell populations were examined. Mature B cells were defined as IgD^{+}, whereas the IgM^{hi} fraction contained a mixture of monocytoid B cells (lymph node equivalents of MZ B cells) and transitional 1 and 2 B cells[31, 32]. Results show no differences in percentage of lymphocytes in either the mesenteric or inguinal lymph nodes of DKO mice when compared to het controls (**Fig. 3.6A, B & C**). Interestingly though, IgM^{hi} B cells, mature B cells and T cells were all reduced in number in DKO mice, especially in the B cell compartment (**Fig. 3.6D, E**).

On day 8 post immunisation with TD antigen NP-CGG, popliteal lymph nodes (the lymph nodes draining the immunised foot) were cut and their histology analysed by immunohistochemistry. As seen in the spleen, TZs and B cell follicles were unaltered (CD3 and IgD staining respectively) (**Fig. 3.7A**). The presence of IgG^{+} B cells in the lymph node medulla in DKO mice indicates class switching is occurring, and $F4/80^{+}$ macrophages are also present only in the medullary regions of both DKO mice and controls. Of those mice that responded to the antigen, dense expression of NP-specific plasma cells was seen in the medullas of LNs (**Fig. 3.7A, B**). NP-binding was also detected in the TZ (presumably due to diffusing antibody, or antibody bound to the reticular cells of the stroma) and also in GCs. Similar to spleen, some NP^{+} cells were seen around GCs in the follicles, most likely representing exiting memory B cells. DKO and het mice both displayed all these same expression patterns. These

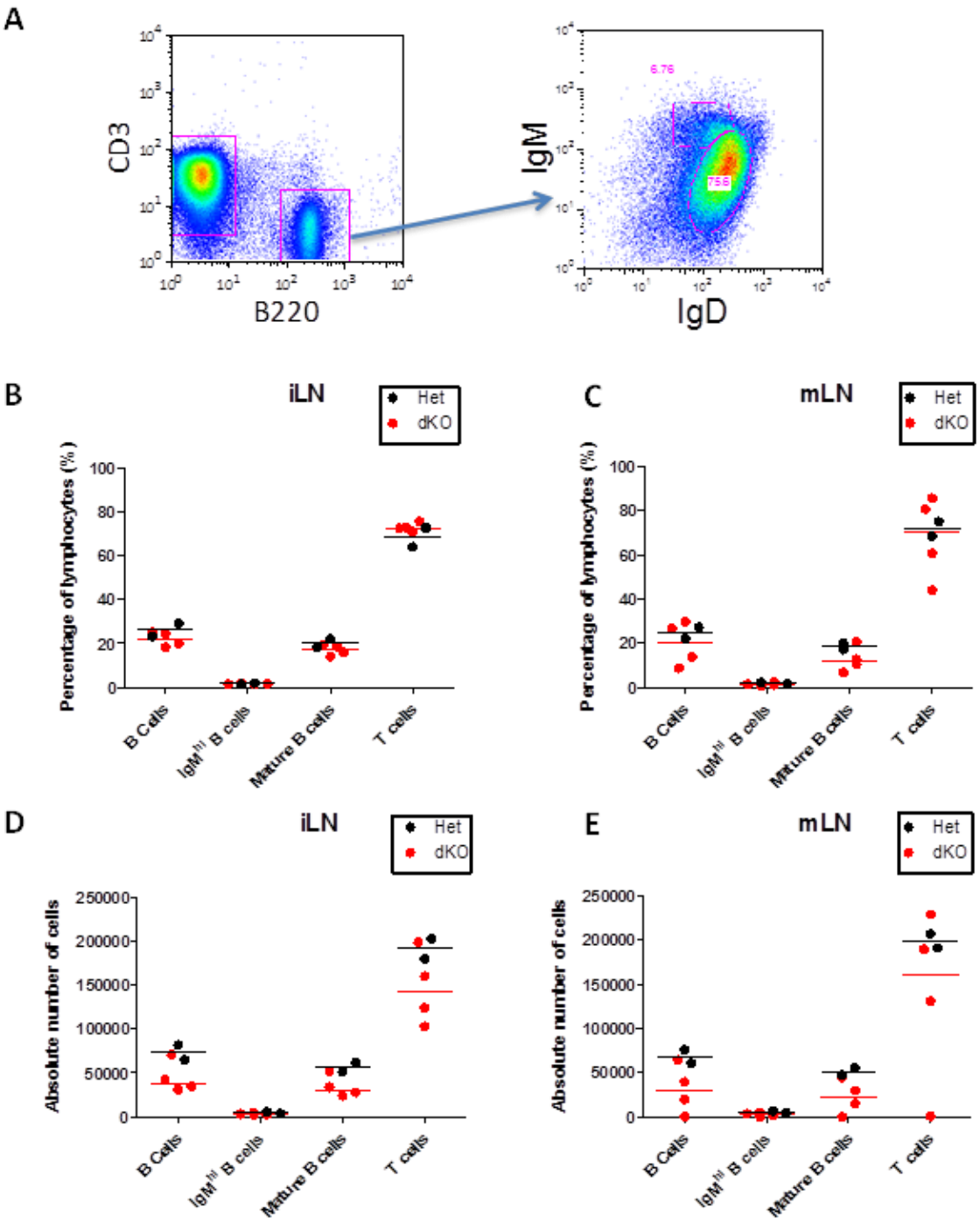

Figure 3.6 – Analysis of the B cell response in the lymph nodes of unimmunised DKO mice.

A – Gating strategy – within the singlet lymphocyte gate, $CD3^+$ cells (T cells) and $B220^+$ cells (B cells) were analysed. In the B cell gate, IgM and IgD were used to distinguish B cell types further. **B –** Percentages of B cells, B cell subtypes and T cells in the inguinal lymph node (iLN – **B**) and the mesenteric lymph node (mLN – **C**). **D –** Absolute cell numbers of the same cell types in iLN (**D**) and mLN (**E**). Lines represent median values. DKO mice (n=4) displayed in red, Het mice (n=2) displayed in black.

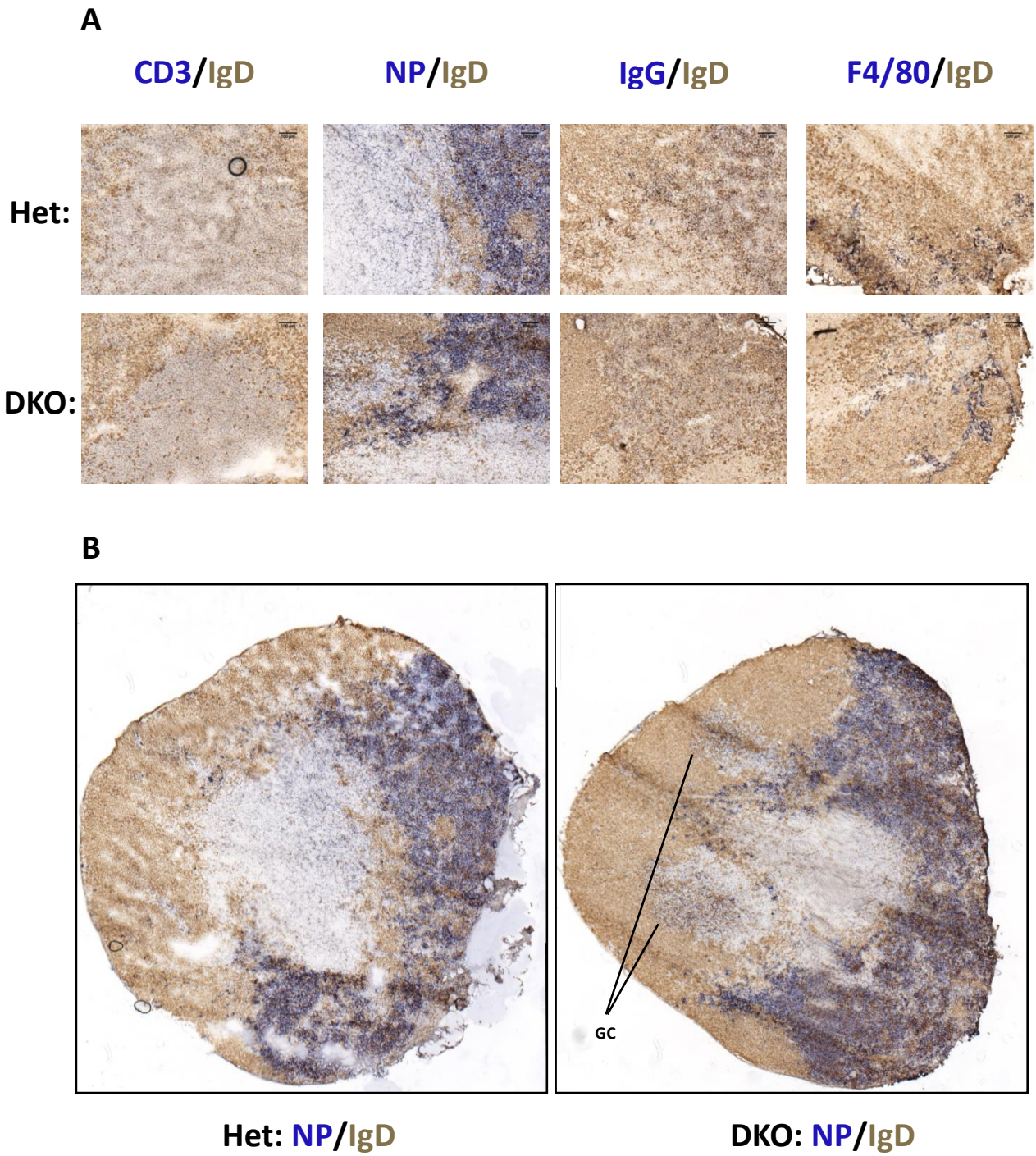

Figure 3.7 – Lymph node architecture in DKO and het control mice.

A – Immunohistochemistry staining of lymph node sections from DKO and het mice immunised with NP-CGG (day 8 p.i.). Sections were stained for CD3, NP, IgG and F4/80 (blue) and IgD (brown). **B –** Whole representative lymph node images of DKO and het samples stained for NP and IgD. 4 het mice and 3 DKOs were used in this experiment.

data revealed apparently normal GC formation and class switching to IgG occur in the LN response to TD antigens in CCRL1/CCRL2 deficient mice.

Interestingly, popliteal lymph nodes from DKO mice were physically smaller and weighed less than control equivalents day 8 p.i. with NP-CGG (**Fig. 3.8A, B**). Consistent with this observation, there were on average less than half the numbers of NP-responder B cells in DKO mice compared to controls (**Fig. 3.8E**). It followed that NP^+ GC B cells (including both DZ and LZ B cells) and NP^+ plasma cells were also reduced in numbers the knockout (**Figs. 3.8C, E**). However, as in the unimmunised mice, there were no differences in percentages of NP^+ responder B cells or their subtypes in DKO mice.

Together these results show no change in the composition of the lymph node, initiating the germinal centre reaction, or undergoing class switching to IgG in DKO mice. However, both pre- and post-immunisation with NP-CGG, B and T cell numbers are reduced.

3.3 – Antibody titres and antibody affinity is unaltered in DKO mice in the TD response

We next wanted to know whether antibody titres and antibody affinity are affected in DKO mice. ELISAs were carried out on serum from unimmunised and immunised mice (day 8 post NP-CGG). Serum was diluted across the ELISA plate and absorbance readings used to calculate relative titres for each mouse (**Fig. 3.9A**). Relative titres of IgM and IgG day 8 p.i. were no different between DKO mice and heterozygous controls, while before immunization antibody titres were undetectable (**Fig. 3.9B**). Total NP-specific IgG1 was detected with NP_{15}, while higher affinity NP-specific IgG1 was detected with NP_2 as only very high affinity IgG would be able to

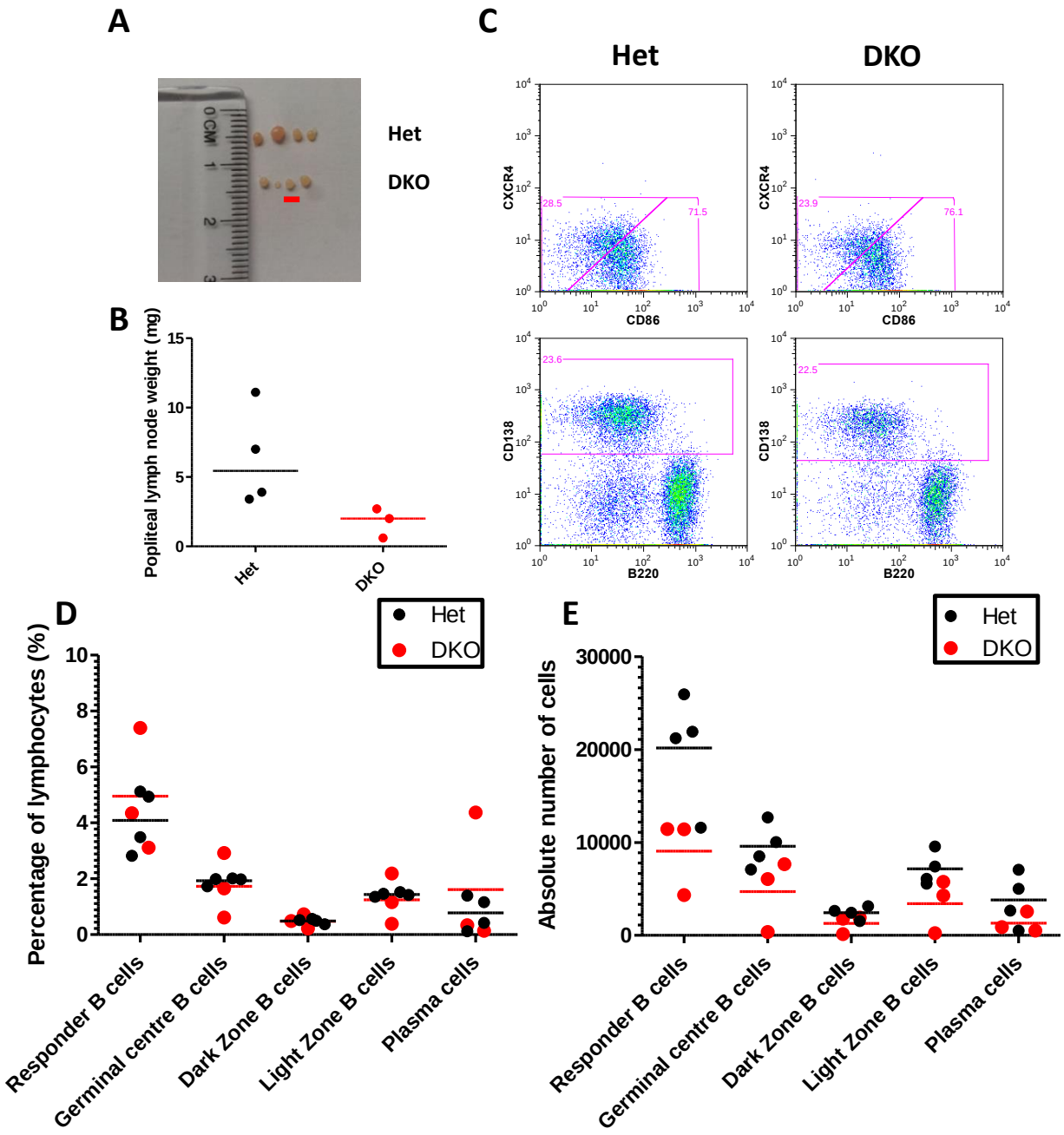

Figure 3.8 – Analysis of the B cell response in the lymph nodes of DKO mice d8 p.i.

A – Photograph comparing size of popliteal lymph nodes of DKO to het controls (red underline shows a LN from a CCRL1-/- CCRL2wt/wt that was originally mistyped as a DKO and therefore excluded from further analysis). **B –** Comparison of popliteal lymph node weights between two groups. **C -** Representative GC B cell (top panel) and plasma cell (bottom panel) plots for het and DKO mice. **D –** Comparison of B cell subtypes in DKOs and controls represented as percentage of lymphocytes (**D**) and cell numbers (**E**) by flow cytometry. Lines represent median values. DKO mice (n=3) displayed in red, Het mice (n=4) displayed in black.

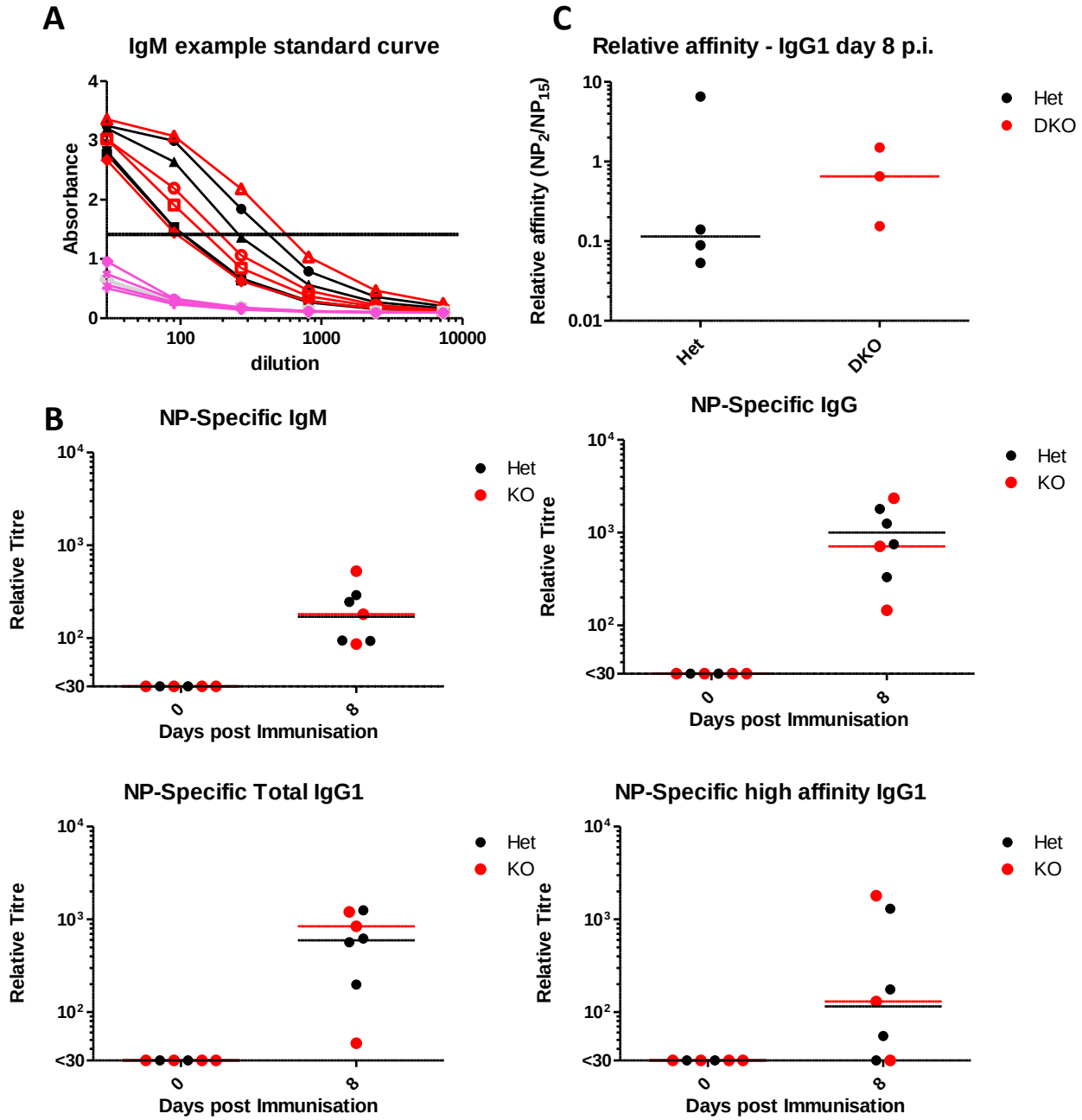

Figure 3.9 – Antibody titres and affinity in DKO mice and controls, unimmunised and day 8 p.i. with NP-CGG.

A – Example standard curve (IgM) of absorbance changing with serum dilution displaying how the relative antibody titres were calculated. Black horizontal line represents chosen absorbance threshold. Red - DKO d8 p.i., black – Het D8 p.i., pink – DKO unimmunised, grey – het unimmunised. **B –** Relative titres for NP-specific IgM, -IgG, -IgG1, and IgG1 of high affinity in DKO and control mice at day 0 (unimmunised) and day 8 post NP-CGG immunisation. **C –** Relative affinity of IgG1 antibody in DKO and control mice day 8 p.i. Calculated by IgG1 high affinity relative titre/ total NP-specific IgG1. Lines indicate median values, red =DKO (n=3) and black = het (n=4).

compete for the two available binding sites. No differences in these antibody titres were detected relative to controls. Lastly, relative affinity of IgG1 was calculated (**Fig. 3.9C**). This too displayed no difference between DKO mice and hets. The combined results therefore suggest no difference in antibody titres or in antibody affinity at day 8 in the TD response, despite reduced NP-specific B cell numbers in the draining lymph node.

3.4 – Preliminary immunofluorescence staining reveals normal subcapsular sinus and medullary macrophage location is normal, and lymph node proliferation patterns are unaltered

In order to see if any other cell types were altered in DKO lymph nodes, preliminary immunofluorescence staining was carried out. We initially wanted to investigate if there were any differences in memory B cell numbers or location by using the combined memory markers CD80 and CD73[33]. Unfortunately, a titration of CD73 was unsuccessful and CD80 staining also did not reveal any significant expression above background in the LN (data not shown). Due to time constrictions these experiments were not taken further.

We also looked at plasma cell location in the popliteal lymph nodes (day 8 p.i. with NP-CGG) using CD138. Plasma cell staining was seen in the medullas of both mice (**Fig. 3.10**). The representative pictures show more intense CD138 staining in the het, but small sample numbers and previous data suggest this is not a real difference. The pictures also show proliferation is occurring throughout both lymph nodes, but mostly in germinal centres. Lastly, CD169 staining revealed that subcapsular sinus macrophages and medullary sinus macrophages were present in both mice[34].

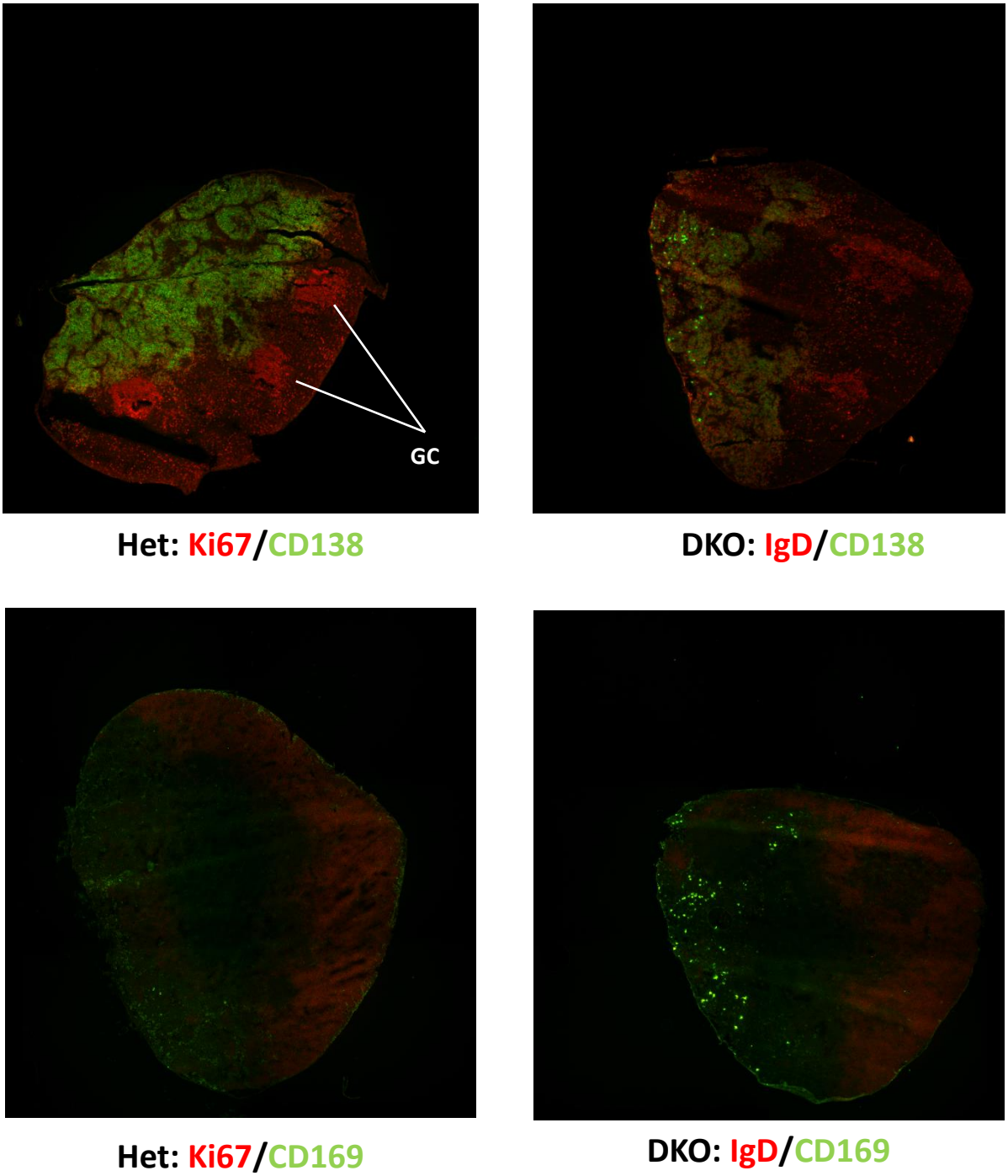

Figure 3.10 – Immunofluorescence staining of whole lymph node sections.

Lymph nodes from DKO and Het mice stained with the following antibodies: anti-IgD -APC and anti-Ki67 Cy-3, anti-CD138 -FITC, and anti-CD169-FITC. Lymph nodes used are day 8 p.i. with NP-CGG (DKO – n=3, Het – n=2).

3.5 – Higher antibody titres are seen in the TI-2 response of DKO mice

To further unravel defects in the B cell response in DKO mice, we next analysed TI-2 responses using the antigen NP-Ficoll. On day 5 of the response, splenocytes were analysed by flow cytometry and the antibody responses in the serum were visualised using ELISAs.

Neither responder cells nor plasma cells were any different in DKO mice compared to WT controls when looked at by percentage of lymphocytes or numbers (**Figs. 3.11C, D**). However, the weight of the whole spleen appeared increased in DKO mice (although the range was fairly large in WT controls) (**Fig. 3.11D**). ELISA results showed that NP specific IgM and IgG3 titres were greater in DKOs (**Fig. 3.11E**). IgM showed a more prominent increase than IgG3 titres, but neither were quite statistically significant ($p=0.1143$ and 0.2 for IgM and IgG3 comparisons respectively). Therefore although there are no differences in the numbers of plasma cells in the spleen, ELISA results indicate class switching takes place, and antibody titres are higher in DKO mice. This suggests that more antibody per plasma cell was being produced, or that antibody production in the DKO plasma cells sets in earlier. Also, other plasma cell populations, such as bone marrow plasma cells, were not analysed and could be help explain these observations.

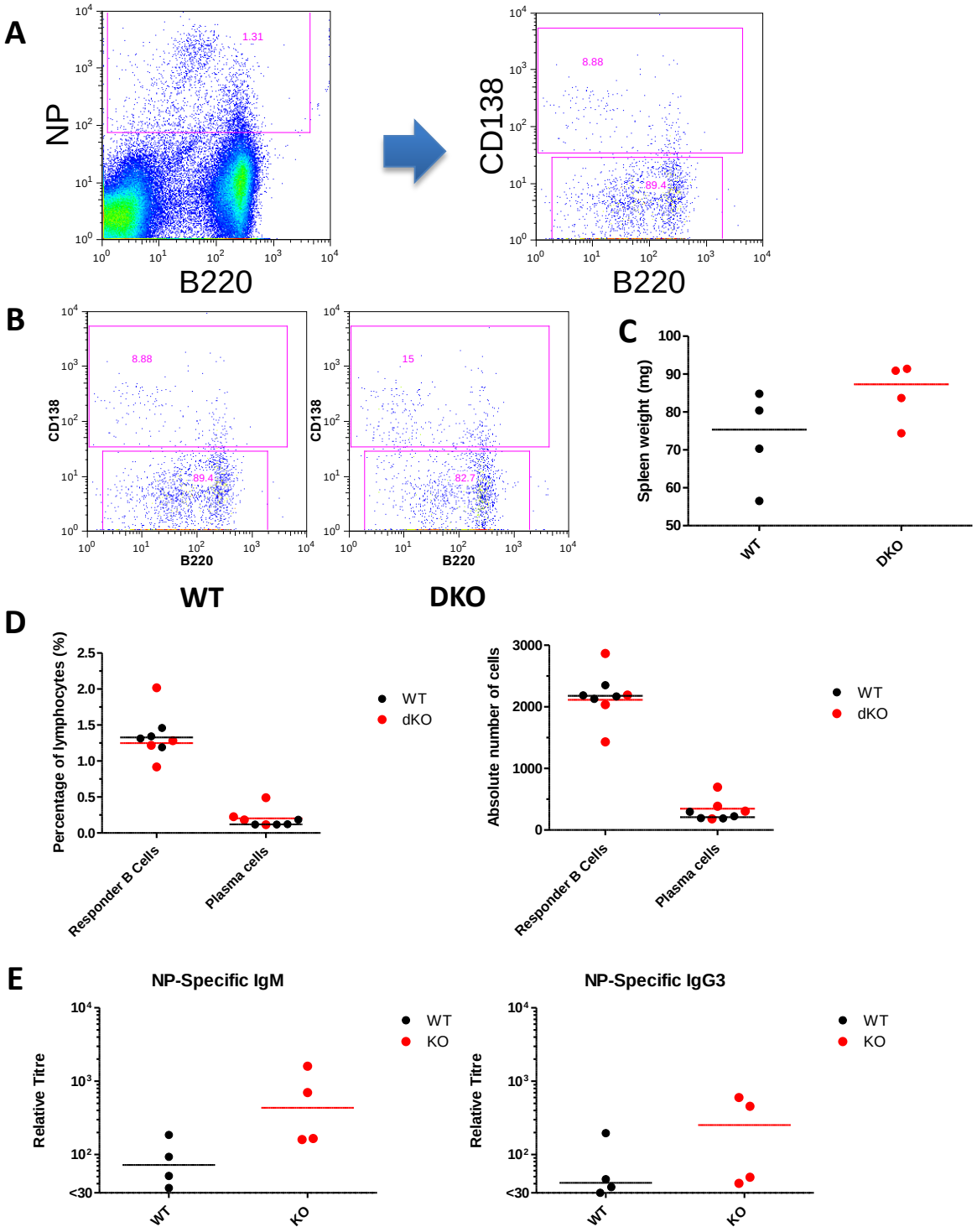

Figure 3.11 – TI-2 responses in DKO mice.

A – Gating strategy used. NP^+ B cells (NP^+B220^+) were gated on and within this population $CD138^+$ plasma cells were analysed (live lymphocyte and singlet gates not shown). **B –** Representative plots from WT and DKO in the B220 responder cell gate. **C –** Spleen weights in the TI-2 response day 5 p.i. **D -** Comparison of NP-responder B cells and NP^+ Plasma cells in DKO and WT control mice day 5post NP-Ficoll immunisation by percentage of lymphocytes (left) and numbers (right). **E –** Relative titres of NP specific IgM and IgG3 as assayed by ELISAs day 5 post NP-Ficoll immunisation. Lines represent median values, red = DKO, black = WT control (both n=4).

4. DISCUSSION

The exact roles of the atypical chemokine receptors CCRL1 and CCRL2 in the B cell response are unclear. CCRL1 binds to and degrades CCR7 ligands CCL19 and CCL21, and our lab has shown CCRL1 is expressed in the GC [Laura Ibanez – unpublished data]. Therefore it has been proposed CCRL1 may be involved in GC homeostasis – by degrading CCL19 and CCL21, CCRL1 could help keep unwanted T cells out of the GC and permit the egress of plasma cells and memory cells. This hypothesis is currently under investigation. In humans CCRL1 has been shown to bind CXCL13, implying a further role in the GC. Whether this is also the case in mice is so far unknown.

The binding partners for CCRL2 are less established: CCL5 and Chemerin have been proposed, along with CCL19. Data from our lab suggests CCRL2 is expressed primarily on plasma cells within the B cell compartment and CCRL2-deficient mice produce more plasma cells and antigen-specific antibody in the TI-2 response. Preliminary results indicate this may be due to increased plasma cell proliferation. There is no major difference in antibody titres in TD responses [Sarah Cook – personal communication].

As CCRL1 and CCRL2 arose by gene duplication, their function may be similar. Therefore it was thought that the lack of a clear phenotype in either of the single knockout mouse strains may be due to a degree of compensation. Thus, a double CCRL1 CCRL2 knockout strain was produced to investigate the phenotype of mice deficient in both receptors.

Overall, a minor phenotype was seen in the DKO mice, but a few interesting observations were made. Unimmunised mice had normal TZs and B cell follicles, marginal zones and red pulp areas in the spleen (**Fig. 3.1A**). However, there were greater numbers of B and T cells in unimmunised DKO mice spleens compared to controls, and within the lymphocyte population both T and B cells were also increased in percentage (**Fig. 3.3**). This was interesting as it suggested another cell type/other cell types were correspondingly decreased. Although results must be interpreted with caution due to small sample numbers and only modest differences in B cell percentages, further investigation is warranted. When the ungated population was analysed this expected decrease was seen, suggesting plasma cells (which can show reduced B220 expression as they mature), DCs or NK cell numbers could be affected. Plasma cells are a possible candidate given the proposed B-cell specific roles of CCRL1 and CCRL2. However the lymphocyte gate used was quite large, so it may also be other non-lymphocyte leukocytes that are behind the decrease. Interestingly, Heinzel et al. showed reduced entry of DC into skin draining lymph nodes in CCRL1-deficient mice, but no differences were reported in the spleens of these mice[17]. A difference in DC homing to the spleen in CCRL1-deficient mice could explain our findings. Staining with additional markers for plasma cells, DCs and additional leukocytes would help explain these results.

Histologically, there were no obvious changes in spleens of DKO mice that were immunised with the TD antigen NP-CGG. GCs were present in DKO mice and plasma cells were produced (**Fig. 3.1B**). Class switching to IgG was also evident in the knockout mice. Plasma cell presence as shown by CD138 staining was not as dense as the NP staining suggests (**Fig. 3.1B – middle panels)**, but it was

suggested this is most likely due to differences in primary antibody affinities. GCs were also suggested to be irregular/rugged in DKO mice. A preliminary blinded quantitative analysis using a subjective measure for ruggedness did not produce substantially different results (**Fig. 3.2**). However, a more objective measure for spatial changes in GC architecture, and larger sample sizes, may change this picture and this needs to be taken further. In both groups combined only three mice had more than 10 GCs in the spleen sections, so larger sample sizes would be needed. The classification of GCs as rugged would also need to be reviewed. A more objective way to measure ruggedness could be the percentage of IgD^+ (brown) cells that were within the boundary of the NP^+ (blue) GC. Also, staining with the GC marker peanut agglutinin (PNA) would allow easier classification of ruggedness. If DKO GCs were found to be more rugged, this would make sense within the proposed model of CCRL1 maintaining GC homeostasis and preventing influx of unwanted cells, possibly by scavenging CXCL13, or by producing a strong CCL19 sink in the GC.

The only observed differences in the TD response in the spleen were a slight decrease in spleen weight and a slight increase in percentage of GC B cells in DKO mice (**Fig. 3.4**). The decrease in spleen weight did not result in any decreases in absolute number of the cell types investigated. The reasons for this are unknown, but it is worth pointing out the average number of responder B cells would be lower if it were not for one het mouse with a very low number (**Fig. 3.4D**). The increase in GC B cells was very slight (**Fig. 3.4C**), but if confirmed would also support a role of CCRL1 in the GC. If CCRL1 is able to bind and degrade CXCL13 in mice, a deficiency in this receptor would cause an increase in available CXCL13, so more B

cells would be attracted to the GC. However, only a tentative conclusion can be made with these results as the GC response in the spleen may not be developed enough at day 8 p.i., and there were difficulties in distinguishing DZ from LZ B cells by flow cytometry. Further repeats at day 8 and a further time point such as day 10 p.i. would allow us to either confirm or reject these trends statistically.

In the LNs, both before and after TD antigen administration, there was a decrease in B and T cell numbers (**Fig. 3.6; 3.8**). There was also a corresponding decrease in weight and size of popliteal LNs at day 8 p.i.. This could imply a role for CCRL1 or CCRL2 in recruiting cells to LNs, though as with other experiments more repeats are needed. This indication would be counter intuitive as CCRL1 is known to degrade CCR7 ligands and so if anything, cellularity of LNs would be expected to increase when this receptor is absent. There may therefore be additional interactions or functions of CCRL1 and CCRL2. Comerford et al. also noticed decrease lymph node cellularity in CCRL1-deficient mice, suggesting lack of CCRL1 is responsible for this phenomenon in our study[16]. Interestingly, our LN results are different to those in the spleen, highlighting the differences in the workings of these two SLOs. The composition of cells present in the LN is not altered.

Histology of DKO mice appears normal, indicating dense NP staining and evidence of class switching in those mice that responded (**Fig. 3.7**). No GCs were seen in the example het LN, but this is most likely due to poor section quality. In both LN and spleen NP^+ cells were seen around the edges of GCs, likely representing memory cells. Data from our lab indicates that memory cells exit the germinal centre and move towards the subcapsular sinus through the follicle [Kai Toellner – personal communication]. We attempted to see if memory B cell chemotaxis was affected in

DKO mice by doing immunofluorescence staining for memory markers CD80 and CD73. Unfortunately staining was unsuccessful and must be repeated in future experiments. If the equipment were available, intravital microscopy could also be used to track memory cell migration in real time. Our immunofluorescence staining here also revealed proliferation was occurring normally in DKO LNs, and $CD169^{+}$ macrophages were present in a distinct pattern around the perimeter of the LN (the subcapsular sinus [**Fig. 3.10**]). This is very similar to immunofluorescence results shown by Satpathy et al[35]. Lastly, in the context of the TD response, ELISAs revealed no difference in antibody titres or IgG1 affinity between DKO and het mice (**Fig. 3.9**).

Within the TI-2 response, no differences were seen in responder B cells or plasma cell compared to controls (**Fig. 3.11**). This is despite an apparent larger weight of DKO spleens. The controls used in these final experiments were WT, not het due to lack of het control mice. While het mice are bred at our own facility, WT mice are bought in from a commercial breeder. This commercial facility is likely to be cleaner than our specific pathogen free facility, and this could explain the slight splenomegaly in the DKO mice. This was not a factor in previous experiments when het littermates were used. Even though responder B cells were not increased in DKOs, and overall lymphocytes were not increased (data not shown) it may have been T cells were increased correspondingly (not analysed). Finally, higher titres of NP-specific IgM and IgG3 were produced by plasma cells from DKO mice (**Fig. 3.11E**). This is in line with data from $CCRL2^{-/-}$ mice [Sarah Cook – personal communication]. However, no corresponding increase in plasma cells conflicts with our labs previous data. These results therefore indicate that plasma cells in CCRL1/CCRL2 deficient mice are

producing more antibody per cell and that additional CCRL1 deficiency may counteract the decrease in plasma cell numbers seen in CCRL2$^{-/-}$ mice alone.

In conclusion, this study provides some valuable preliminary data on the roles of these receptors in antibody responses, but in many cases further supporting data are needed. Key B cell types were present in the DKO in their expected locations. DKO spleen analysis showed increases in B and T cells before immunisation but no difference in these cells after immunisation with NP-CGG. Conversely, LN B cell populations were decreased both before and after NP-CGG immunisation. The TD response revealed no difference in NP-specific antibody titres, whereas both IgM and IgG3 were increased in the TI-2 response. Although no mechanism can be inferred from this data, interesting avenues of further study include looking into GC shape (ruggedness), increases in GC B cell populations and memory cell chemotaxis in these DKO mice. It appears that the effects of these two receptors are disparate, rather than similar as originally thought, and there appear to be no compensatory overlapping functions that would have been revealed in the DKO mice. CCRL1 deficiency is probably responsible for the potential rugedness of GCs, while CCRL2 is more likely behind the increased antibody titres in the TI-2 response (supported by recent data from our lab). Therefore the mouse model used in this study may well be complicating the picture rather than simplifying it as the effects of deficiencies in both receptors are compounded. Continuing the studies of single CCRL1 and CCRL2 knockout mice are the obvious way to address this issue, and could be vital in fully understanding B cell migration and function in SLOs, and thus in modifying the B cell response.

References

1. Mebius, R. & Kraal, G. Structure and function of the spleen. *Nat. Rev. Immunol.* **5**, 606-616 (2005).

2. von Andrian, U. & Mempel, T. Homing and cellular traffic in lymph nodes. *Nat. Rev. Immunol.* **3**, 867-878 (2003).

3. Gonzalez, S. F. *et al*. Trafficking of B cell Antigen in Lymph Nodes. *Annu. Rev. Immunol.* **29**, 215-233 (2011).

4. MacLennan, I. *et al*. Extrafollicular antibody responses. *Immunol. Rev.* **194**, 8-18 (2003).

5. Allen, C. D. C., Okada, T. & Cyster, J. G. Germinal-center organization and cellular dynamics. *Immunity* **27**, 190-202 (2007).

6. Nutt, S. L. & Tarlinton, D. M. Germinal center B and follicular helper T cells: siblings, cousins or just good friends? *Nat. Immunol.* **12**, 472-477 (2011).

7. Capolunghi, F., Rosado, M. M., Sinibaldi, M., Aranburu, A. & Carsetti, R. Why do we need IgM memory B cells? *Immunol. Lett.* **152**, 114-120 (2013).

8. Broxmeyer, H. E. Chemokines in hematopoiesis. *Curr. Opin. Hematol.* **15**, 49-58 (2008).

9. Baggiolini, M., Dewald, B. & Moser, B. Human chemokines: An update. *Annu. Rev. Immunol.* **15**, 675-705 (1997).

10. Fernandez, E. & Lolis, E. Structure junction, and inhibition of chemokines. *Annu. Rev. Pharmacol. Toxicol.* **42**, 469-499 (2002).

11. Rot, A. & von Andrian, U. Chemokines in innate and adaptive host defense: Basic chemokinese grammar for immune cells. *Annu. Rev. Immunol.* **22**, 891-928 (2004).

12. Mebius, R. & Kraal, G. Structure and function of the spleen. *Nat. Rev. Immunol.* **5**, 606-616 (2005).

13. Green, J. A. & Cyster, J. G. S1PR2 links germinal center confinement and growth regulation. *Immunol. Rev.* **247**, 36-51 (2012).

14. Wang, H. *et al*. The CXCR7 chemokine receptor promotes B-cell retention in the splenic marginal zone and serves as a sink for CXCL12. *Blood* **119**, 465-468 (2012).

15. Nibbs, R. J. B. & Graham, G. J. Immune regulation by atypical chemokine receptors. *Nat. Rev. Immunol.* **13**, 815-829 (2013).

16. Ulvmar, M. H., Hub, E. & Rot, A. Atypical chemokine receptors. *Exp. Cell Res.* **317**, 556-568 (2011).

17. Heinzel, K., Benz, C. & Bleul, C. C. A silent chemokine receptor regulates steady-state leukocyte homing in vivo. *Proc. Natl. Acad. Sci. U. S. A.* **104**, 8421-8426 (2007).

18. Malhotra, D. *et al*. Transcriptional profiling of stroma from inflamed and resting lymph nodes defines immunological hallmarks. *Nat. Immunol.* **13**, 499-U107 (2012).

19. Bunting, M. D. *et al*. CCX-CKR deficiency alters thymic stroma impairing thymocyte development and promoting autoimmunity. *Blood* **121**, 118-128 (2013).

20. Gosling, J. *et al*. Cutting edge: Identification of a novel chemokine receptor that binds dendritic cell- and T cell-active chemokines including ELC, SLC, and TECK. *J. Immunol.* **164**, 2851-2856 (2000).

21. Townson, J. & Nibbs, R. Characterization of mouse CCX-CKR, a receptor for the lymphocyte-attracting chemokines TECK/mCCL25, SLC/mCCL21 and MIP-3 beta/mCCL19: comparison to human CCX-CKR. *Eur. J. Immunol.* **32**, 1230-1241 (2002).

22. Comerford, I. *et al*. The atypical chemokine receptor CCX-CKR scavenges homeostatic chemokines in circulation and tissues and suppresses Th17 responses. *Blood* **116**, 4130-4140 (2010).

23. Biber, K., Zuurman, M., Homan, H. & Boddeke, H. Expression of L-CCR in HEK 293 cells reveals functional responses to CCL2, CCL5, CCL7, and CCL8. *J. Leukoc. Biol.* **74**, 243-251 (2003).

24. Zabel, B. A. *et al*. Mast cell-expressed orphan receptor CCRL2 binds chemerin and is required for optimal induction of IgE-mediated passive cutaneous anaphylaxis. *J. Exp. Med.* **205**, 2207-2220 (2008).

25. Leick, M. *et al*. CCL19 is a specific ligand of the constitutively recycling atypical human chemokine receptor CRAM-B. *Immunology* **129**, 536-546 (2010).

26. Yoshimura, T. & Oppenheim, J. J. Chemokine-like receptor 1 (CMKLR1) and chemokine (C-C motif) receptor-like 2 (CCRL2); Two multifunctional receptors with unusual properties. *Exp. Cell Res.* **317**, 674-684 (2011).

27. Otero, K. *et al*. Nonredundant role of CCRL2 in lung dendritic cell trafficking. *Blood* **116**, 2942-2949 (2010).

28. Monnier, J. *et al*. Expression, Regulation, and Function of Atypical Chemerin Receptor CCRL2 on Endothelial Cells. *J. Immunol.* **189**, 956-967 (2012).

29. Pillai, S., Cariappa, A. & Moran, S. Marginal zone B cells. *Annu. Rev. Immunol.* **23**, 161-196 (2005).

30. Victora, G. D. *et al*. Germinal Center Dynamics Revealed by Multiphoton Microscopy with a Photoactivatable Fluorescent Reporter. *Cell* **143**, 592-605 (2010).

31. Tierens, A., Delabie, J., Michiels, L., Vandenberghe, P. & De Wolf-Peeters, C. Marginal-zone B cells in the human lymph node and spleen show somatic hypermutations and display clonal expansion. *Blood* **93**, 226-234 (1999).

32. Loder, F. *et al*. B cell development in the spleen takes place in discrete steps and is determined by the quality of B cell receptor-derived signals. *J. Exp. Med.* **190**, 75-89 (1999).

33. Tomayko, M. M., Steinel, N. C., Anderson, S. M. & Shlomchik, M. J. Cutting Edge: Hierarchy of Maturity of Murine Memory B Cell Subsets. *J. Immunol.* **185**, 7146-7150 (2010).

34. Gray, E. E. & Cyster, J. G. Lymph Node Macrophages. *J. Innate Immun.* **4**, 424-436 (2012).

35. Satpathy, A. T. *et al*. Zbtb46 expression distinguishes classical dendritic cells and their committed progenitors from other immune lineages. *J. Exp. Med.* **209**, 1135-1152 (2012).

PROJECT B:

THE BATTLE OF THE CARS: CD28 COSTIMULATORY ENDODOMAINS ENDOW T CELLS WITH MORE ROBUST EFFECTOR FUNCTIONS *IN VITRO* COMPARED TO THEIR 4-1BB COUNTERPARTS

Ben Wiggins – MRes (Masters in Biomedical Research)

Principal Investigator: Dr Steven Lee

Supervised by: Steven Lee and Alan Zhuang

27/01/2014 – 25/04/2014

This project is submitted in partial fulfilment of the requirements for the award of the MRes

School of Cancer Sciences,

Vincent Drive,

University of Birmingham,

Edgbaston,

Birmingham,

B15 2TT

MRC Medical Research Council

Acknowledgements:

Thank you to Steve Lee for giving me a chance to work in such an interesting field of cancer research, and all his help and support. Thank you to Baksho Kaul for all the hours she has given up helping me and her endless assistance. Lastly, thank you to the rest of the lab for their help and for being so welcoming.

Table of contents:

List of Tables and Figures:

ABSTRACT:

Adoptive transfer T cell therapy involves the *ex vivo* expansion of T cells followed by reinfusion to a patient to treat disease. These T cells can be engineered to express chimeric antigen receptors (CARs) that combine MHC-independent antigen recognition with T cell effector functions. Second generation CARs encompass a costimulatory endodomain to enhance T cell activation and survival. So far, there have been conflicting reports concerning whether CD28-containing CARs or 4-1BB-containing CARs provide T cells with favourable responses. Therefore, this investigation aimed to compare these two constructs for the *in vitro* functional T cell output they provide. T cells were retrovirally transduced with either construct, both of which recognise CLEC14A – a tumour vasculature antigen, and their transduction efficiencies, proliferation and IFN-γ production analysed. CD28-CAR$^+$ T cells showed slightly enhanced transduction efficiencies when compared to 4-1BB-CAR$^+$ T cells. Furthermore, CD28-CAR$^+$ T cells produced far superior IFN-γ and degranulation responses, but 4-1BB-CAR$^+$ T cells showed a greater resistance to apoptosis. Together, these data suggest the CD28-CAR is favourable, showing greater IFN-γ and cytotoxic responses, despite the greater propensity for apoptosis. Further work will allow an optimum CAR to be designed for future use in the treatment of human cancers.

List of abbreviations:

4-1BB-CAR^{+} T cells - T cells transduced to express a 2nd generation CAR containing 4-1BB
AICD – Activation-induced cell death
APC – Antigen presenting cell
Bcl-XL - B-cell lymphoma-extra large
CAR – Chimeric antigen receptor
CD – Cluster of differentiation
CD28-CAR^{+} T cells – T cells transduced to express a 2nd generation CAR containing CD28
CD40L – CD40 Ligand
CLEC14A - C-type lectin domain family 14, member A
CLL – Chronic lymphocytic leukaemia
DC – Dendritic cell
GM-CSF - Granulocyte-macrophage colony-stimulating factor
IFN-γ – Interferon-gamma
IL – Interleukin
LAG-3 - Lymphocyte-activation gene 3
MDSC - myeloid-derived suppressor cell
MHC - Major Histocompatibility Complex
NK cell – Natural Killer cell
NKT cell – Natural Killer T cell
PBMC – Peripheral blood mononucleocyte
PD-1 - Programmed cell death-1
PD-L1 - Programmed cell death ligand 1
RAG2 - recombinase activating gene-2
TAA – Tumour associated antigen
TCR – T cell receptor
TIM3 - T-cell immunoglobulin domain and mucin domain 3
TNF-α – Tumour necrosis factor-α
TRAIL - TNF-related apoptosis-inducing ligand
T_{REG} – Regulatory T cell
TSA – Tumour-specific antigen

1. INTRODUCTION

1.1 - Cancer Immunoediting

It is well established that the immune response influences the development of many cancer types. Effector leukocytes have the ability to recognize tumour-specific antigens (TSAs) and eliminate the tumour cells before cancer becomes apparent. This process is referred to as cancer immunosurveillance[1]. However, cancer still develops in immunocompetent individuals, and there is strong evidence showing that the same process can also promote cancer growth. Eliminating the most immunogenic cancer cells may result in the survival of the least immunogenic variants, potentially allowing the establishment of more resilient cancer cells. Evidence for this comes from studies that demonstrate tumours transferred from immunocompromised mice into wild-type mice are rejected more readily than tumours transplanted from wild-type origin[2-5]. Taking the actions of the immune system on both preventing and promoting cancer growth into account, the hypothesis of cancer immunoediting was proposed[5]. Cancer immunoediting can be broken down into three distinct phases – the elimination phase, the equilibrium phase, and the escape phase[5].

The elimination phase is synonymous with the term cancer immunosurveillance; describing the destruction of tumour cells and thus preventing malignancy[1]. This is not a new concept; many studies have described an increased susceptibility of immunocompromised animals to a variety of cancers in various mouse models of tumour induction. Likewise in human studies, higher frequencies of malignancies are seen in immunodeficient individuals. This includes patients with acquired immunodeficiency syndrome or on immunosuppressive treatments[1].

Both the innate and adaptive arms of the immune system are involved in the anti-cancer response. The response begins when innate immune cells such as natural killer (NK) cells, Natural killer T (NKT) cells, γδ T cells and macrophages are recruited by proinflammatory cytokines and chemokines that either originate from the tumour itself, or are released due to the local destruction caused by characteristic stromal remodelling. Recognition of the tumour then occurs, and the cytokine interferon-gamma (IFN-γ) is produced. This in turn induces chemokine-mediated recruitment of more innate immune cells, and by a variety of local positive feedback mechanisms, the amount of IFN-γ produced is amplified. IFN-γ stops tumour growth by inhibiting both angiogenesis and proliferation, and also causes apoptosis[5]. Furthermore, IFN-γ induces TNF-related apoptosis-inducing ligand- (TRAIL) dependent tumour cell killing by macrophages, and perforin-dependent killing by NK cells[5]. The tumour antigens that are released as a result of tumour cell death are taken up by activated dendritic cells (DCs). These DCs migrate to the draining lymph node and present their antigen to naïve $CD4^+$ and $CD8^+$ T cells. Tumour-specific T cells are activated in turn, and migrate to the tumour site. Here they recognise tumour-associated antigens (TAAs) and cause destruction of the tumour cells as well as amplifying the whole process through the release of more IFN-γ[5] (process reviewed in more detail in REF 5).

Despite the efficacy of the immune response against cancer, the least immunogenic tumour cells may survive, allowing for their persistence. This is because the immune attack exerts a strong selection pressure on the heterogeneous tumour population, resulting in the survival of only those mutant cells that can withstand the response[5]. These variants enter the equilibrium phase where tumour cells are still present, but

net outgrowth is prevented by the immune system. This phase can continue asymptomatically for the lifetime of a patient[1].

The final stage of cancer immunoediting is termed the escape phase. This occurs when tumour variants acquire mutations that provide them with the means to escape recognition completely, or with resistance to immune attack. It is at this phase when tumours become clinically detectable[5]. Tumour cells can circumvent the immune response in a great many ways, including the downregulation of the major histocompatibility complex (MHC) molecules required for T cell recognition, and the upregulation of anti-apoptotic molecules such as B-cell lymphoma-extra large (Bcl-XL). Tumour cells can also acquire mutations leading to the expression of molecules that directly kill T cells, for example programmed cell death ligand 1 (PD-L1) or Fas ligand. On top of this, tumour cells can secrete a variety of anti-inflammatory cytokines and other factors that dampen the immune response and recruit regulatory cells such as myeloid-derived suppressor cells (MDSCs) and regulatory T cells (T_{REGs}) to the tumour site, which in turn inhibit the immune response further[1] (Reviewed in REF 1).

1.2- The role of T cells in targeting cancers

T cells have shown to be vital in the recognition and elimination of various cancers. Mice deficient for the recombinase activating gene-2 (RAG2), lack T cells, and studies have shown these mice are more susceptible to both chemically induced and spontaneous tumours when compared to wild type mice[2]. Furthermore, in mice lacking αβ T cells or γδ T cells, susceptibility to chemically induced and injected tumours is increased[7] . Both $CD8^+$ (cytotoxic) and $CD4^+$ (helper) T cells have roles in this tumour cell rejection. $CD8^+$ T cells can degranulate, releasing cytotoxic mediators, following recognition of TAAs that are displayed on MHC class I

molecules on the tumour cell surface, but can also contribute to tumour cell killing by IFN-γ production. $CD4^+$ T helper 1 (T_H1) cells promote $CD8^+$ T cell recruitment, and also provide IL-2 signals to facilitate $CD8^+$ T cell survival, as well as producing IFN-γ and tumour necrosis factor-α (TNF-α). Furthermore, they can enhance the activation of DCs via CD40-CD40L interactions, thus allowing the priming of more $CD8^+$ T cells[8, 9]. More recently, studies have shown some $CD4^+$ T cells can develop cytotoxic activity and kill tumour cell targets directly[10, 11].

However, as eluded to above, T cells do not always succeed at destroying the cancerous cells completely, allowing for immune evasion and outgrowth. This may be because many TAAs are derived from self-proteins that are aberrantly expressed, and so central and peripheral tolerance mechanisms that prevent targeting of self-tissues only allow T cells with low T cell avidity for these antigens to survive and respond[12]. Also, tumour infiltrating T cells may undergo T cell exhaustion, and the tumour cells may acquire mutations that allow for downregulation of antigen presentation, T cell suppression, and T cell apoptosis[8]. Therefore methods by which the T cell response to cancers can be enhanced are needed.

1.3- Adoptive T cell transfer therapy for the treatment of cancers

In order to utilise and enhance the natural immune response against cancers, immunologists have turned to adoptive T cell transfer therapies. This process involves the isolation of T cells from a patient and their expansion in culture. The cells are then reinfused back to the patient in order to treat disease[8, 12]. Isolated T cells are often cultured with IL-2 to facilitate their expansion, before those T cells with the desired specificities and differentiation states can be selected and transferred back to the patient[8]. Host lymphodepletion can be carried out to improve transferred

T cell survival and engraftment, and co-administration regimens of cytokines such as IL-2, IL-15 or IL-7 have been explored to enhance the anti-tumour response[13].

This treatment has distinct advantages over more conventional treatments. It is minimally invasive unlike surgery, and should be more controlled and specific when compared to traditional chemotherapy options based on targeting all dividing cells. Furthermore, evidence suggests that adoptive T cell transfer therapy is much more efficacious than therapeutic vaccines in achieving complete tumour regression[8].

Isolated T cells can also be engineered to express receptors of desired specificities. This is usually done by retroviral or lentiviral transduction techniques whereby a viral carrier transports the transgene of interest into the T cell and causes its integration into the genome – resulting in stable expression. Two main types of engineered T cells have been explored – those expressing αβ T cell receptors (TCRs); or those expressing CARs (chimeric antigen receptors) [12].

1.4 - Chimeric antigen receptors (CARs)

1.4.1 - Introduction to CARs

CARs are comprised of an intracellular TCR signalling domain fused to the antigen binding domain of an antibody[12]. CARs combine the potent effector functions of T cells with the high antigen affinity of antibodies, making for a robust and powerful anti-tumour response. First generation CARs consist of extracellular variable heavy and light chain fragments connected by a linker sequence, a transmembrane domain, and the intracellular CD3ζ signalling domain of the TCR complex. Second generation CARs also include a costimulatory endodomain fused to the CD3ζ, while third generation CARs contain two costimulatory endodomains (**Fig 1.1**). These domains are derived from the costimulatory molecules CD28, 4-1BB (CD137) or OX40

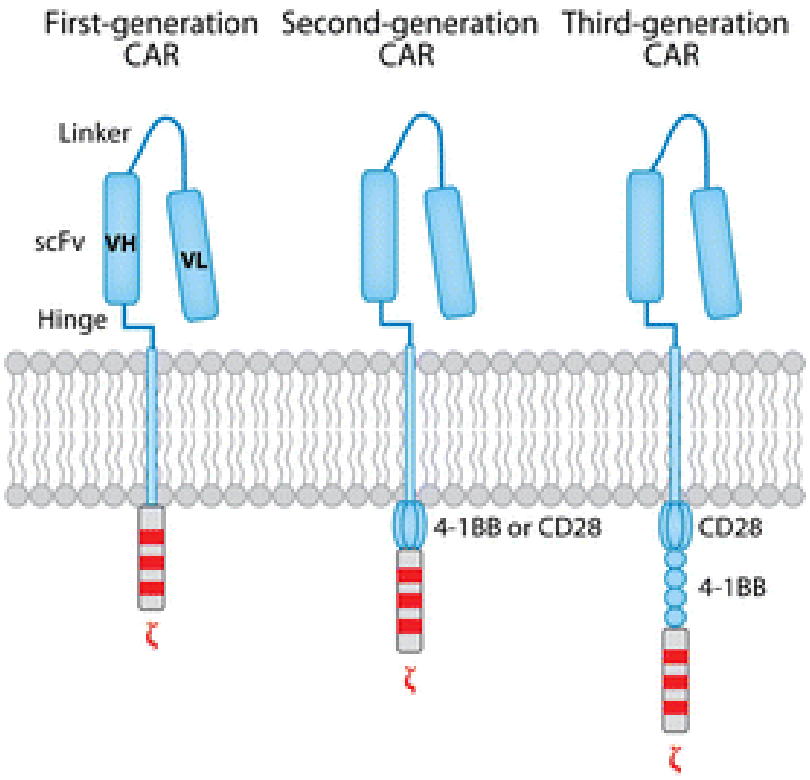

Figure 2.1– First, second and third generation CAR constructs.

First generation CARs are comprised of antibody variable light and heavy chain domains, connected by a linker sequence, a hinge domain, a transmembrane domain and an intracellular CD3ζ domain. The extracellular antibody domain (single chain variable fragment – scFv) provides high affinity, non-MHC restricted antigen recognition, while the hinge domain allows for flexibility of this binding region. The CD3ζ signalling domain mediates the transformation of antigen recognition into signalling pathways and T cell effector function. Second generation CARs also incorporate a costimulatory endodomain, such as 4-1BB or CD28 that increase T cell activation and survival. More recently, third generation CARs have been developed that include two costimulatory endodomains. VH – variable heavy chain, VL – variable light chain, ζ – CD3ζ domain. Figure taken from REF 13.

(CD134). Studies have shown that the inclusion of costimulatory endodomains results in greatly enhanced T cell survival and expansion, and prevents T cells undergoing functional unresponsiveness (anergy), when compared to first generation CARs in both mouse and human studies[13-20].

1.4.2 - Benefits and drawbacks of CARs in cancer immunotherapy

Transducing T cells with CAR constructs as opposed to αβTCR constructs can have a number of advantages. CARs can function in a non-MHC restricted manner that is not dependent on antigen processing and presentation[8, 12]. In this way they can maintain their effectiveness against tumour cells that have downregulated MHC molecules, and theoretically all patients can be treated regardless of their HLA haplotype. Secondly, CARs recognize target molecules with far greater affinity than αβTCRs, and thus overcome T cell tolerance mechanisms that require high affinity ligation to permit T cell activation[12]. The drawbacks of using CARs include the fact they contain murine sequences in their ligand-binding domains, making these neoepitopes potential targets of the immune system. Additionally, although CARs are not MHC restricted, this does mean they are unable to recognize intracellular antigens. This means a smaller range of target antigens are available, and the cell surface targets could also be subject to downregulation as part of the tumour immune evasion process[12]. However, it is thought the benefits of using CARs outweigh the limitations; hence the large number of ongoing clinical trials involving CARs to target cancers.

1.4.3 - The role of costimulatory molecules in T cell activation

The costimulatory molecule CD28 is required for full T cell activation. CD28 on the T cell surface binds to CD80 or CD86 which are both expressed by antigen presenting cells (APCs). This provides a second signal alongside the MHC-peptide-TCR

interaction. CD28 ligation prevents the T cell undergoing anergy; and enhances the T cell response, cytokine production, proliferation and survival[21]. It is worth noting that although CD28 signalling is vital in naïve T cell activation, it is thought to be less important in effector and memory T cell responses[17].

Similarly, 4-1BB is expressed on T cells and interacts with its ligand 4-1BB ligand (4-1BBL) that is expressed by activated APCs[22]. This interaction also constitutes an important costimulatory pathway for T cells, acting to increase T cell expansion, cytokine production and cytotoxic effector functions [23]. Studies have demonstrated that 4-1BB-mediated costimulation can be both CD28-dependent and -independent[22, 24]. Independently of CD28 signalling, 4-1BB ligation can prevent activation-induced cell death (AICD)[25], but also 4-1BB can act synergistically with CD28 to lower the threshold for CD28 ligation needed to sustain proliferation and IL-2 production in mice[22, 26, 27]. In $CD4^+$ T cells, 4-1BB signalling also regulates CD28 costimulation to skew towards IFN-γ producing T_H1 cells that have shown to be important in anti-cancer responses[26]. However, cytotoxic $CD8^+$ T cells are preferentially expanded by 4-1BB signalling when compared to $CD4^+$ T cells[28]. Additionally, early studies suggest a role for 4-1BB in memory T cell induction and maintenance[29, 30]. This is interesting as memory T cells have been suggested to be better candidates than effector T cells for adoptive transfer as they survive longer *in vivo*[13]. Finally, it has been shown that agonistic anti-4-1BB antibodies can completely eradicate tumours in mice[31, 32].

1.4.4 - Second generation CARs – comparing CD28 and 4-1BB costimulatory endodomains

The use of second generation CARs has shown great potential as a feasible and effective cancer treatment. As mentioned, second generation CARs show much improved responses when compared to first generation CARs. Mouse studies revealed CD28-CAR$^+$ T cells showed strong proliferative responses and produced high levels of effector cytokines *in vivo*[17, 33, 34]. In clinical trials there have also been successes. Savoldo et al. demonstrated CD28-CAR$^+$ T cells expand and persist better than 1st generation CAR$^+$ T cells of the same specificity in B cell non-Hodgkins lymphoma patients, despite seeing no clinical responses [15, 34]. However, Kochenderfer et al. observed clinical remission in 75% of treated patients with advanced B cell malignancies after transfer of CD28-CAR$^+$ T cells[35], and in a separate trial, an even better complete response rate of 88% was reported[36]. Various other promising clinical trials with CD28-CARs are ongoing in patients with B cell malignancies (reviewed in REFS 13, 34).

Finney et al. were the first to engineer secondary CARs to express 4-1BB endodomains. Their study revealed human T cells transduced with 4-1BB-containing CARs showed enhanced survival, proliferation and cytokine production compared to T cells transduced with 1st generation CARs. However, the production of IL-2, IFN-γ, TNF-α and granulocyte-macrophage colony-stimulating factor (GM-CSF) by 4-1BB-CAR$^+$ T cells was significantly lower than CD28-containing CAR-T cells, and there was no difference in antigen specific cell lysis when comparing cells transduced with 4-1BB containing constructs to those transduced with 1st generation CARs in this particular study[17]. Notwithstanding, although another study suggested CD28-CAR$^+$ T cells show slightly more proliferation, they also showed less IFN-γ and GM-CSF

production compared to 4-1BB-CAR$^+$ T cells [37]. Additionally, a comparison of 4-1BB and CD28-containing constructs in a mouse model of acute lymphoblastic leukaemia indicated the former endowed T cells with more favourable responses. 4-1BB-CAR$^+$ T cells had a greater antileukemic efficacy and longer in vivo persistence than their CD28-containing counterparts[38]. Furthermore, T cells containing the 4-1BB construct were able to proliferate independently of CAR engagement. This has never been observed in CD28-containing CARs[34, 38]. It has also been reported that the incorporation of 4-1BB into the CAR construct increases multifunctional cytokine production of T cells *in vivo* [16], but other studies dispute this[33].

The 4-1BB construct has also been shown to have therapeutic applicability. Porter et al. conducted an autologous adoptive transfer with T cells engineered to express 4-1BB into a chronic lymphocytic leukaemia (CLL) patient. This led to complete remission at the time of their publication[39]. A Follow up study by the same laboratory with a larger study group reported potent anti-tumour activity, long term persistence and 'unprecedented and massive in vivo expansion' of transferred 4-1BB-CAR$^+$ T cells in CLL patients[40]. A third study by this group also reported highly potent responses in CLL patients when engineered 4-1BB-CAR$^+$ cells were transferred, supported by B cell aplasia, decreased plasma cells and hypogammaglobulinemia. The cells expanded over 1000-fold post transfer, and some transferred cells even persisted as memory CAR$^+$ T cells. Two of three patients in the study achieved complete remission[41]. Despite these encouraging findings, exhaustive comparison of 4-1BB- containing CARs with CD28-containing CARs in human T cells has not yet been done (although a comparative clinical trial is currently in progress [clinicaltrails.gov NCT01044069] [19, 42].

1.5 - Study aims

Many of these clinical trials use CARs that recognise CD20 – an antigen expressed only on B cells, and thus useful in treating B cell malignancies. However, solid tumours have proved more challenging targets for adoptive transfer therapy. This is due to a lack of tumour specific antigens, as well as due to the propensity of tumour cells to mutate to allow immune evasion – for example through decreasing antigen expression through MHC on the cell surface. Therefore, an alternative targeting mechanism is needed. One such alternative is through targeting the tumour vasculature. A recent study has reported that expression of the C-type lectin CLEC14a is greatly increased on tumour vasculature compared to healthy blood vessels[43]. This molecule is therefore potentially an excellent tumour target.

Our lab uses 5 CAR constructs (CRT1-5) that are engineered to recognise CLEC14a. Our previous data with human T cells transduced with second generation CD28-containing CARs show greatly enhanced IFN-γ responses, proliferation and cytotoxic activity when compared to both mock controls and first generation CARs with the same specificity. Furthermore, those cells transduced with CD28-CARs also persist for a prolonged period in mice, and significantly slow tumour growth in the Lewis lung carcinoma model [Steve Lee – personal communication]. The lab has recently engineered a new second generation construct with the 4-1BB costimulatory domain in place of the CD28 domain. Thus, given the discrepancies in the literature, this study aimed to see whether the CD28-CAR or the 4-1BB-CAR provided T cells with better proliferation and greater effector functions *in vitro*. T cells were transduced to express one of the CARs containing either CD28 or 4-1BB, and their transduction efficiencies, proliferation, cytokine production and cytotoxicity were compared.

2. MATERIALS AND METHODS

2.1 – List of reagents and media

Reagent/Media	Components
PBS	1 PBS tablet [Oxoid, Basingstoke, UK] dissolved to total volume of 100mls with distilled water
PBS/BSA	PBS containing 2% (w/v) Bovine Serum Albumin (BSA)[Sigma]
Complete RPMI	RPMI (Roswell Park Memorial Institute) 1640 [Sigma-Aldrich, Gillingham, UK], 1% L-Glutamine (2mM)[Gibco], 100U/ml penicillin [Sigma], 100U/ml streptomycin [Sigma], 10% Fetal bovine serum (FBS) [Biosera, Ringmer, UK]
T cell media (TCM)	Complete RPMI containing 1% Human Serum [Biosera, Ringmer, UK]
Transfection media	DMEM (Dulbecco's Modified Eagle Medium)[Sigma], 1% L-glutamine (2mM)[Gibco], 10% Fetal bovine serum (FBS) [Biosera, Ringmer, UK]
Complete DMEM	Transfection media containing 100U/ml penicillin [Sigma], 100U/ml streptomycin [Sigma]
MACS buffer	PBS, 2mM ethylenediaminetetraacetic acid (EDTA)[Sigma], 0.5% BSA [Sigma]
Coating buffer	0.1M Na_2HPO_4 - adjusted to pH9 with addition of 0.1M NaH_2PO_4
Blocking buffer	PBS containing 1% (w/v) BSA [Sigma], and 0.05% (v/v) Tween-20 [Sigma], sterile filtered with 0.45µm filter

Table 2.1 - List of cell culture media and other reagents used in this investigation

2.2 – T cell transfection and transduction

Phoenix A cell culture:

Phoenix A cells [Nolan lab, Stanford University] were thawed and cultured at 37^{O}C, 5%CO_2 in complete DMEM until 50-80% confluent. Media was removed and cells washed once with PBS before 1X Trypsin-EDTA [Gibco, UK] was added for approximately 2 minutes to bring cells to a single cell suspension. Complete DMEM was added and cells centrifuged (355g, 5 minutes). Cells were then resuspended in

transfection media, counted with a haemocytometer, and seeded into seven T25 flasks [Corning, NY, USA] – 2 x 10^6 cells in a volume of 10mls per flask. These flasks were cultured overnight (37^OC, 5%CO_2).

Transfection:

7 sterile 1.5µl microcentrifuge tubes were prepared – 4 for each of the vectors used and 3 for mock tranfection controls. The second generation CAR-containing plasmids used were as follows: CRT3 CD28 and CRT5 CD28 [both generated by Zhuang, X.]; and CRT3 4-1BB and CRT5 4-1BB [both generated by Clarke, L]. 600µl Optimem [Gibco, UK] was added to each tube, alongside 3µg relevant plasmid DNA. 3µl of retroviral vector pCL ampho (1µg/ml) [Imgenex, San Diego, USA] was added to the mixtures containing plasmids to maximise recombinant retrovirus titres. 24µl PEI stock (1mg/ml) [Sigma-Aldrich, Gillingham, UK] was then added to all tubes. These mixtures were vortexed and incubated at room temperature for 10 minutes. Meanwhile, Phoenix A cell culture media was removed and 3.5ml fresh transfection media added. After 10 minutes, the plasmid mixtures were added to the relevant Phoenix A cells, mixed well and placed into incubation (37^OC, 5% CO_2). 24 hours later, media was removed and fresh transfection media added before cells were placed back in the incubator for a further 24 hours.

Transduction:

Peripheral blood mononucleocytes (PBMCs) were counted with a haemocytometer and resuspended at 1 X 10^6 cells/ml in TCM. Cells were stimulated with 30ng OKT3 [eBioscience, San Diego, USA], 30ng anti-CD28 [R&D systems, Oxfordshire, UK], and 100U/ml IL-2 [Novartis, UK]; placed into T100 flasks and incubated overnight (37^OC, 5% CO_2).

For the transduction procedure, 6 well non-tissue culture treated plates were coated with 2mls/well retronectin (30µg/ml) [Clontech, Saint-Germain-en-Laye, France] for 3 hours. After removal of the retronectin, wells were blocked with 2.5mls sterile PBS/BSA for 30 minutes, and then washed three times with PBS. Phoenix A cell culture supernatants were harvested and centrifuged (400g, 5 minutes) to pellet any residual phoenix A cells. Supernatants were transferred to the retronectin-coated wells and centrifuged (2000g, 120 minutes, $32^{O}C$) to allow spinfection. Meanwhile, the stimulated T cells were counted again, centrifuged (355g, 5 minutes) and resuspended in TCM containing 100U/ml IL-2 to a concentration of 1×10^6 cells/ml. These cells were placed in the incubator for 15 minutes to recover. After spinfection, retronectin-coated plates were washed once with PBS, and 5×10^6 PBMCs added to each well. Plates were spun once more (355g, 5 minutes) and incubated overnight. The following day, cells were transferred to tissue culture treated 6 well plates and a further 3 mls TCM (containing 100U/ml IL-2) was added to each well.

2.3 – Cell culture

Transduced T cell cultures were examined regularly, and fresh TCM(+ 100U/ml IL-2) added, or cells split when necessary. Some cells were cultured on CLEC14A-coated plates: non-tissue culture treated plates were incubated with 2mls of human CLEC14a-Fc [produced by by Zhuang, X.] (1µg/ml – dissolved in PBS) for 3 hours at $37^{O}C$, 5% CO_2, washed once with PBS, and T cells added. Cells were cultured in CLEC-14a-coated plates for up to a week, after which time they were transferred to 6-well tissue culture treated plates.

2.4 – Flow cytometry

Surface Staining:

For single colour staining, 200µl of cells were transferred to FACS tubes, 2mls of MACS buffer added and the cells centrifuged for 3 minutes, 411g. Supernatant was removed and cells were resuspended with relevant fluorescently labelled antibodies for 30 mins in the dark at $4^{O}C$. Cells were washed with MACS buffer as before (2mls MACS added and centrifuged 3 minutes, 411g) and resuspended in 200µl MACS buffer ready for flow cytometric analysis. Similarly, for multicolour staining, cells were transferred to 96 well V-bottom plates, washed in MACS buffer, incubated with relevant antibodies for 30 mins on ice, washed once more, and then transferred to FACS tubes for analysis. If fixing was required, cells were resuspended in 1% Paraformaldehyde in MACS buffer. Compensation beads were prepared by the addition of one drop of positive and one drop of negative compensation beads into 100µl of MACS buffer, addition of the relevant antibody, incubation at $4^{O}C$ for 30 minutes, addition of a further 2 mls MACS buffer and then centrifugation (302g, 10 minutes). Analysis was carried out on either a BD biosciences Accuri C6 flow cytometer, using Accuri CFlow Plus v.1.0.227.4 software, or a BD Biosciences LSR II flow cytometer, using BD FACSDiva v.8.0 software. Data were analysed offline using FlowJo v.7.6.5 software and BD FACSDiva v.8.0 software, and data presented using Graphpad Prism v.5 software.

CFSE assay:

Maxisorp 96-well plates (Nunc) were coated with human CLEC14a-Fc (1µg/ml in PBS), or human Fc fragment [Bethyl, Montgomery, USA] (1µg/ml in PBS) and

incubated at 37^{O}C for 5 hours. T cells were counted with a haemocytometer and the required volumes aliquoted into falcon tubes before each transduced T cell line was diluted with mock transfected cells in order to equalize the percentages of transduced cells for all samples. Cells were centrifuged (411g, 5 minutes) and resuspended at a concentration of 1 x 10^6 cells/ml in a 1μM solution of CFSE (carboxyl fluorescent succinimidyl ester) [Invitrogen, UK] in PBS. Samples were initially incubated for 15 minutes (37^{O}C, 5% CO_2), before they were centrifuged (411g, 5 minutes) and resuspended in TCM at 1 x 10^6 cells/ml and incubated at 37^{O}C, 5% CO_2 for a further 30 minutes. Cells were washed twice (first in RPMI, then TCM – both times at 411g, 3 minutes) and resuspended in TCM + IL-2 (10U/ml).

After the 5-hour coating step, Maxisorp plates were washed with TCM, and then 3 x 10^5 cells added to the wells. T cells cultured with 600U/ml IL-2 were included as positive controls. Plates were incubated for 4-6 days. Cells were then transferred to FACS tubes and washed once in MACS buffer (411g, 3 mins). A 1/100 dilution of vital dye [Life Technologies, UK] was added to each tube, and tubes incubated in the dark at room temperature for 20 minutes. Following this, surface staining and flow cytometric analysis was carried out as above.

Degranulation assay:

Human umbilical vein endothelial cells (HUVECs) [courtesy of Cawkwell L.] were washed gently with PBS before 1X Trypsin-EDTA was added to dissociate cells. One wash was carried out with TCM (centrifuged at 355g, 5 minutes), then HUVECs were resuspended in TCM and counted with a haemocytometer. 10,000 HUVECs per well

were added to a 96-well flat bottom plate. T cells were also counted with a haemocytometer and 5 x 10^4 cells added to the HUVECs. Well volumes were made up to 200µl with TCM. Equivalent wells of T cells alone were also set up. First 5µl anti-CD107a-FITC antibody and then 5µl of monensin (0.25mM in TCM)[Sigma Aldrich, Gillingham, UK] were added to each well and mixed thoroughly. Plates were centrifuged for 3 mins, 210g and incubated for 12 hours (37^{O}C, 5% CO_2). Additional surface staining and analysis was carried out as above.

Apoptosis assay:

Cells placed into hypoxia were cultured in a 96 well plate at a density of 1.5 x 10^6 cells/ml, before being placed into a hypoxia chamber set to 1% O_2, 37^{O}C for 2 days. Equivalent controls were cultured at the same density under normoxia (37^{O}C, 5% CO_2). Surface staining was carried out using the FITC Annexin V apoptosis detection kit II [BD Biosciences, San Jose, USA]. Cells were washed twice with MACS buffer and resuspended in 1X Binding buffer at a concentration of 1 x 10^6 cells/ml.100µl of cell suspensions were transferred to FACS tubes and 5µl of each the Annexin V and propidium iodide (PI) antibodies were added. For compensations, some cells were stained with Annexin V only, or PI only. Cells were incubated for 15 mins in the dark, and 400µl binding buffer added to each tube. Cells were analysed by flow cytometry using the BD Biosciences LSR II flow cytometer and analysed with BD FACSDiva v.8.0 software. Data was presented using Graphpad Prism v.5 software.

2.5 – IFN-γ sandwich enzyme-linked immunosorbent assay (ELISA)

Maxisorp 96-well plates (Nunc) were coated with human CLEC14a-Fc (1µg/ml in PBS), mouse CLEC14a-Fc [Produced by Noy, P.] (1µg/ml in PBS) or human Fc fragment (1µg/ml in PBS) for 3 hours at 37^{O}C. Plates were washed once with PBS and T cells at correct concentrations added. T cells were prepared as follows. Each T cell line was counted and aliquots diluted with mock to balance the percentages of transduced cells (as previously in CFSE assay). T cells were washed with RPMI (spun 411g, 5 mins) and resuspended at the required concentration in TCM before being transferred to the Maxisorp plates. The plate was centrifuged (411g, 3 mins) and incubated for 16-24 hours at 37^{O}C, 5% CO_2. On the same day, a new Maxisorp 96-well plate was coated with anti-human γIFN antibody (0.75µg/ml) [Thermo Scientific, MA, USA] diluted in coating buffer, sealed with Nescofilm and placed at 4^{O}C overnight.

The following day, primary antibody was flicked off and blotted, before the plate was blocked with blocking buffer for 2 hours (200µl/well) at room temperature. Plates were washed 4 times with PBS containing 0.05% (v/v) Tween-20 (PBS/Tween), then 50µl of T cells or recombinant human IFN-γ standards [Sigma-Aldrich, Gillingham, UK] added to relevant wells. IFN-γ standard concentrations used were 20000, 10000, 5000, 2500, 1250, 625, 312.5 and 0 pg/ml. Plates were incubated at room temperature for 3 hours, after which 4 more washes with PBS/Tween were carried out and 50µl of biotinylated anti-IFN-γ antibody (0.75µg/ml) [Thermo Scientific, MA, USA] was added to each well. After an hour at room temperature, plates were washed 4 times with PBS/Tween, and Extra-avidin peroxidase [Sigma] diluted 1/1000 in blocking buffer was added – 50µl per well. After a 30 minute incubation period at room temperature, plates were washed 8 times with PBS/Tween and 50µl of TMB

substrate [Invitrogen, UK] was added to each well. Approximately 20 minutes later, when the colour had developed, the reaction was stopped with 1M Phosphoric acid (50µl/well). Absorbance at 450nm was measured on a Bio-Rad 680 plate reader using Bio-Rad Microplate manager v.5.2.1 software. The IFN-γ concentrations were determined from the standard curve (calculations performed with Microsoft Excel 2007 software) and these were subtracted from the responses against Fc alone. Data were presented using Graphpad Prism v.5 software.

2.6 – Antibody list

Specificity	Conjugation	Species/ Isotype	Final Dilution	Experiment	Company
Human CD34	PE-Cy5	Mouse IgG1	1/50	Flow cytometry	BD Pharmingen
Human CD4	PE-TR	Mouse IgG1	1/100	Flow cytometry	Beckman Coulter
Human CD8	eFluor450	Mouse IgG1	1/50	Flow cytometry	eBioscience
Human CD8	PE-TR	Mouse IgG1	1/50	Flow cytometry	Beckman Coulter
Human CD107a	FITC	Mouse IgG1	1/20	Flow cytometry	BD Pharmingen
Human Annexin V	FITC	-	1/20	Flow cytometry	BD Biosciences
Human IFN-γ	-	Mouse IgG1	1/1360	ELISA	Thermo Scientific
Human IFN-γ	Biotin	Mouse IgG1	1/1333	ELISA	Thermo Scientific

Table 2.2 - List of antibodies used in this study. PE - Phycoerythrin, Cy5 – Cyanine 5, TR – Texas Red, FITC - Fluorescein isothiocyanate.

3. RESULTS

3.1 – CD28 CARs show slightly better T cell transduction efficiencies, and show greatly enhanced CLEC14A-mediated expansion in culture compared to their 4-1BB containing counterparts

T cell expression of the CARs was enabled by retroviral transduction mediated by Phoenix A cells. On day 4 post transduction, T cells were assayed to determine the efficiency of transduction of the CAR in the T cell population. This was achieved through flow cytometric detection with a fluorescently-labelled anti-CD34 antibody, as each CAR vector contains a truncated CD34 molecule. As CD34 is not present on T cells naturally, this method allows for specific detection of transduced T cells.

Across 4 separate transduction procedures transduction efficiency was fairly consistent and generally between 10 and 20% of lymphocytes (**Fig. 3.1B**). The exception is the third transduction, which resulted in far lower efficiencies (ranging between 1.55 – 2%). The reasons for this are unclear, but may be due to overconfluency of Phoenix A cells during the transfection procedure.

Upon comparing CD28-containing constructs with 4-1BB-containing constructs, the mean percentages of transduced cells were slightly lower in the latter. Although the mean difference is slight, in two out of three of the repeats, the efficiency of transduction in T cells containing CD28-containing CARs (CAR-CD28$^+$ T cells) was clearly higher than their 4-1BB counterparts (CAR-4-1BB$^+$ T cells). Therefore, in conclusion, both 4-1BB and CD28-containing constructs are capable of transduction, but marginally higher efficiency is seen with CD28.

Additionally, T cells were cultured on plates coated with human CLEC14A-Fc in attempt to selectively expand those cells that expressed the CLEC14A specific CAR.

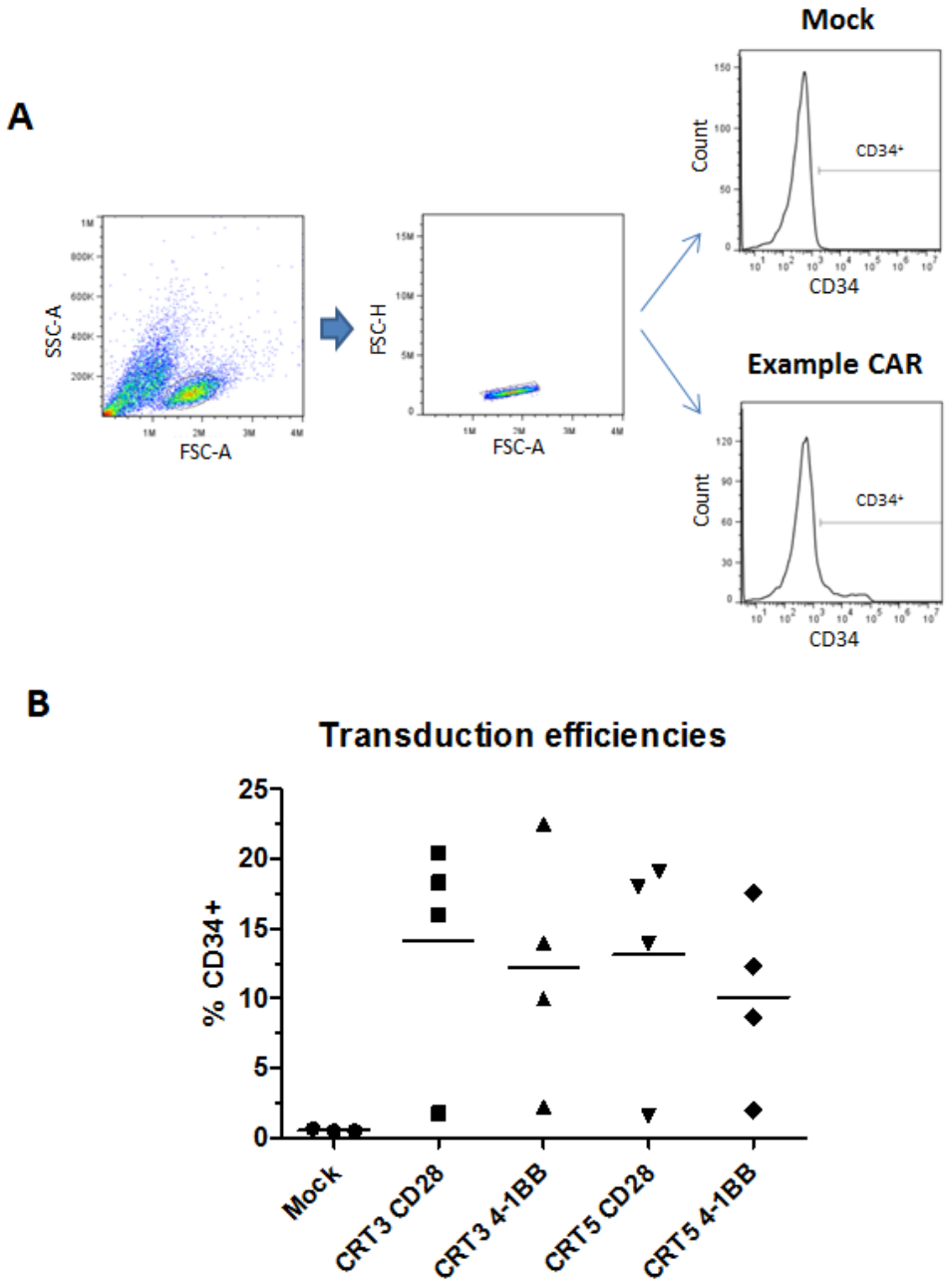

Figure 3.1 – Efficiency of transduction of each CAR-construct.

A – Gating strategy used. First lymphocytes were gated on according to their forward and side scatter parameters (FSC-A and SSC-A respectively). Next the area of forward scatter (FSC-A) and the height of forward scatter profiles (FSC-H) were plotted for the gated population to omit everything but single cells. Finally a histogram of PE-Cy5 (CD34) signal was plotted. The gate determining $CD34^+$ cells was set according to the mock-transduced PE-Cy5 histogram profile (mock-transduced cells – upper, example CAR transduction – lower. **B – Transduction efficiencies of 4 CARs in T cells.** Graph shows the efficiency of the transduction procedure as the percentage of $CD34^+$ cells of singlet lymphocytes. Each T cell line, and mock-transduced cells are plotted. Data points from all experiments are shown (n=4) and line represent mean values.

CAR-CD28^{+} T cells showed marked expansion after coating with CLEC14A, whereas the percentage of CAR-4-1BB^{+} T cells did not increase at all (**Fig. 3.2**). This pattern was consistent in other repeats.

3.2 – Minimal antigen-specific proliferative responses observed to plate-bound CLEC14A

Next, we wanted to see if there was any difference in proliferative responses to CLEC14A by CAR-4-1BB^{+} T cells when compared to CAR-CD28^{+} T cells. When cells were stained on day 4 after culture with CLEC14A-coated plates, (**Fig.3.3B –** top panel) CD8^{+} T cells transduced with CRT5-CD28 displayed the greatest proliferative response. For T cells expressing this construct, proliferation against CLEC14A was increased compared to proliferation against Fc only control plates, suggesting some proliferation was specific. For the other constructs, the percentage of divided cells following CLEC14A stimulation is not increased when compared to Fc controls, showing little antigen-specific proliferation has occurred. The same pattern could be seen in CD8^{-} cells (assumed to be CD4^{+} T cells), with only T cells transduced with CRT5-CD28 showing any antigen-specific proliferation. When the CD8^{+} T cells were compared to CD8^{-} cells overall, levels of proliferation were higher in the CD8^{+} population for cells cultured with CLEC14A and Fc controls, while the cells cultured with high levels of IL-2 showed similar proliferation in both subsets.

When cells were stained on day 6 after culture (**Fig. 3.3B –** bottom panel), the overall proliferative responses were lower than those on day 4. The greatest proliferative response seen was in CD8^{+} T cells transduced with CRT3-CD28, but as the response to Fc alone was greater, this proliferation cannot be considered specific. The only specific proliferation seen was in T cells transduced with CRT3-CD28 in the

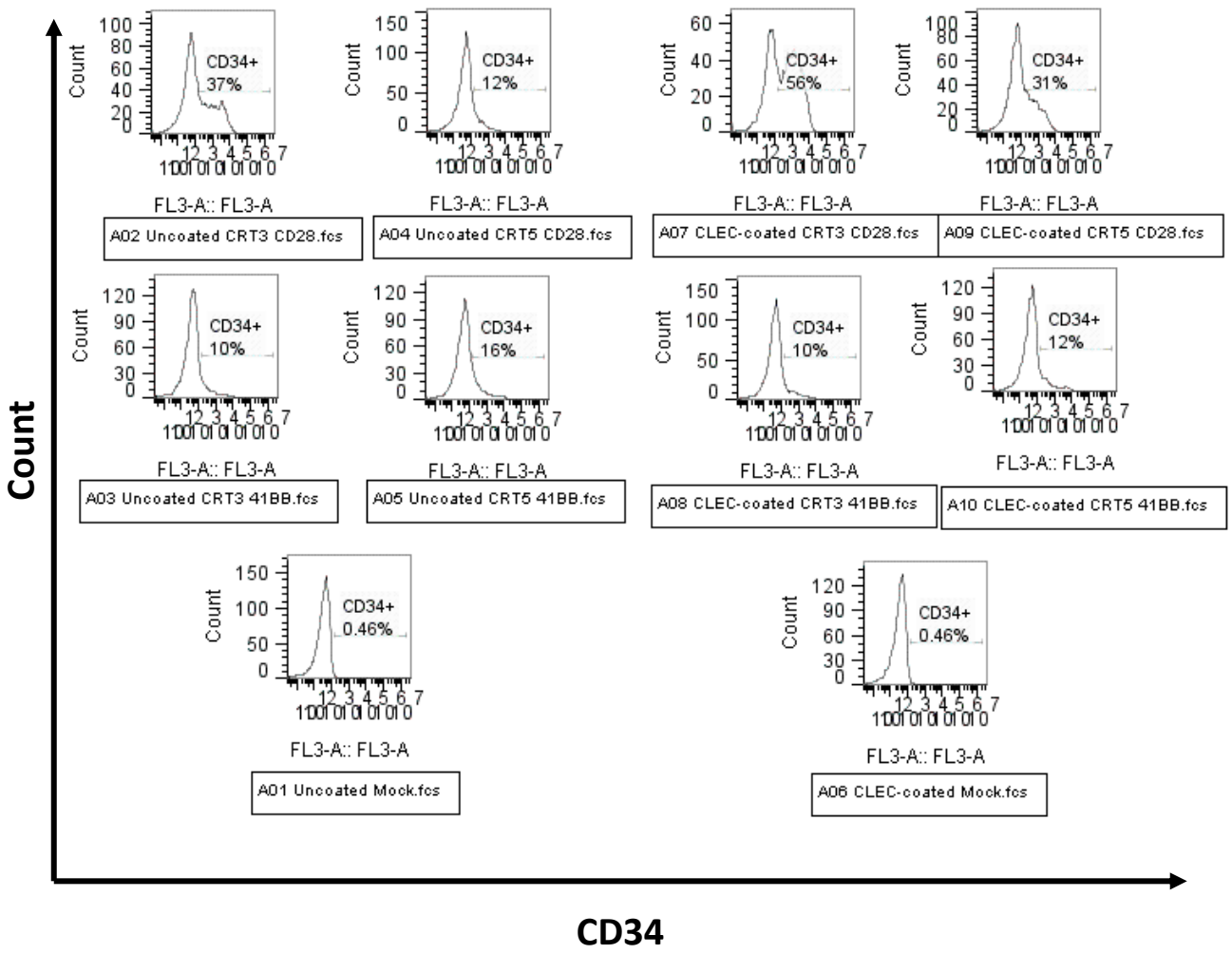

Figure 3.2 – Transduction efficiencies before and after culture on human CLEC14A-coated plates.

This example shows the transduction efficiencies measured in T cells that had been cultured with human CLEC14A-Fc (right panel) or standard tissue culture plates (left panel). T cells were cultured on CLEC14-A coated plates for 6 days. Analysis of T cells cultured on non-coated plates was done on the same day to enable fair comparison. First row shows CD28 constructs second row shows 4-1BB constructs and bottom row shows mock controls. Percentages of $CD34^+$ cells are given with each plot.

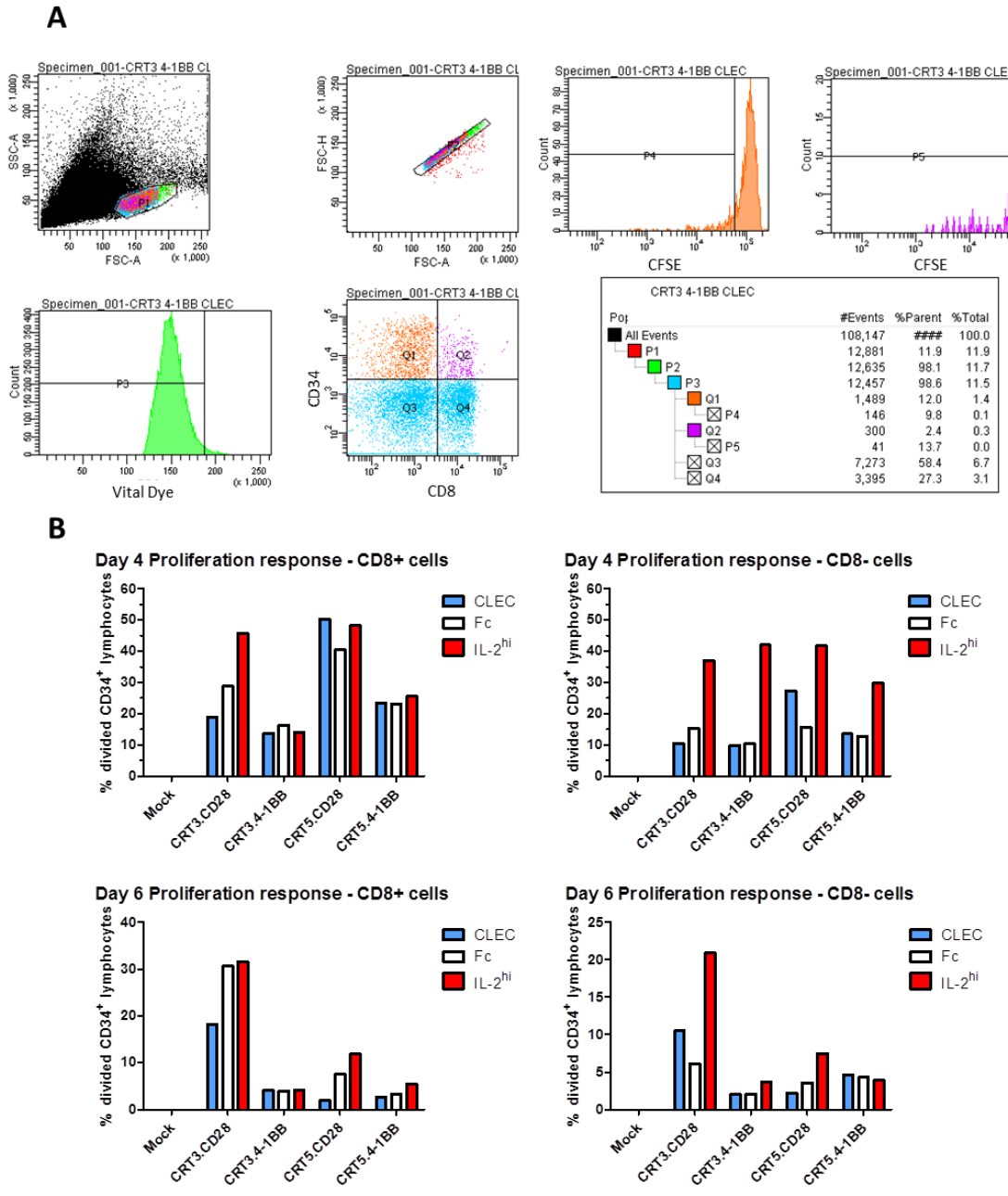

Figure 3.3 – Proliferative responses to plate-bound human CLEC14A. A – Gating strategy.

First singlet lymphocytes were gated on as described as previously. Next, vital dye^{hi} cells were excluded to remove dead cells from analysis. Quadrant gates were drawn on remaining cells such that the percentages of $CD34^+CD8^+$ and $CD34^+CD8^-$ cells could be analysed for CFSE incorporation and plotted. The dialogue box illustrates gating hierarchy. **B – Proliferation responses at days 4 and 6 post culture with human CLEC14A.** Graphs show the percentage of singlet $CD34^+$ lymphocytes that have undergone cell division in each T cell line. Top and bottom panels represent the response at days 4 and 6 post culture respectively (each day was the result of a separate experiment using separate donors). Left panels show $CD8^+$ cells, while right panels show $CD8^-$ cells. Key: blue bars=T cells cultured with human CLEC14A-Fc, white bars=T cells cultured with Fc only, red bars= T cells cultured with a high concentration of IL-2 (600U/ml). N=1.

$CD8^-$ fraction. Similarly to day 4, more cell division was observed in $CD8^+$ T cells as a whole than in $CD8^-$ cells. Overall, these results show T cells transduced with either CD28 or 4-1BB constructs fail to produce a substantial antigen-specific proliferative response to plate bound CLEC14A. However, this could conceivably be due to the assay failing as far more specific proliferation was expected in these cells.

3.3 – CD28 constructs endow T cells with superior IFN-γ production in response to CLEC14A than their 4-1BB-containing counterparts

The effector cytokine IFN-γ is produced by $CD4^+$ T_H1 T cells and $CD8^+$ T cells and is important in the anti-tumour response[44]. To this end, we measured the IFN-γ production by the transduced T cells in response to different concentrations of plate-bound CLEC14A using ELISA methodology. The responses of CAR-$CD28^+$ T cells were compared to CAR-4-$1BB^+$ T cells. Both T cells that had been cultured in tissue-culture treated plates, and T cells that had been previously cultured in CLEC14A-coated plates were used in these experiments.

T cells expressing CRT3 and CRT5 CD28 constructs both display a strong IFN-γ response, far higher than their corresponding 4-1BB-CAR^+ engineered T cells (**Fig. 3.4A**). The first repeat resulted in CRT3 $CD28^+$ T cells producing the most IFN-γ, whereas in the second experiment CRT5 $CD28^+$ T cells produced higher IFN-γ levels. The responses of either of the 4-1BB-construct expressing cell populations were not significant, showing no increase from the production by mock-transduced cells. Therefore in both experiments where T cells that were previously cultured without CLEC14A, CD28 constructs perform consistently better than 4-1BB in inducing IFN-γ production in T cells. CRT5 $CD28^+$ T cells and CRT3 $CD28^+$ T cells may be able to produce similar levels of IFN-γ at high CLEC14A concentrations

A

Repeat 1:

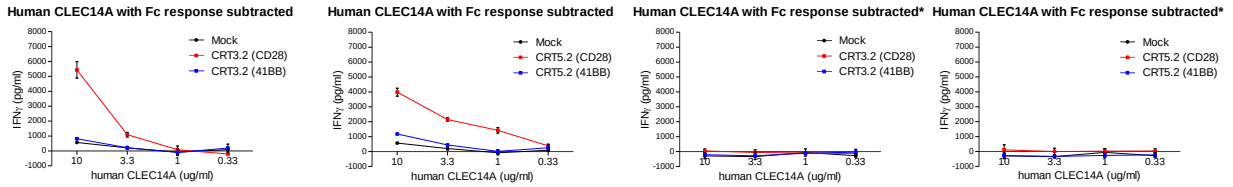

Repeat 2:

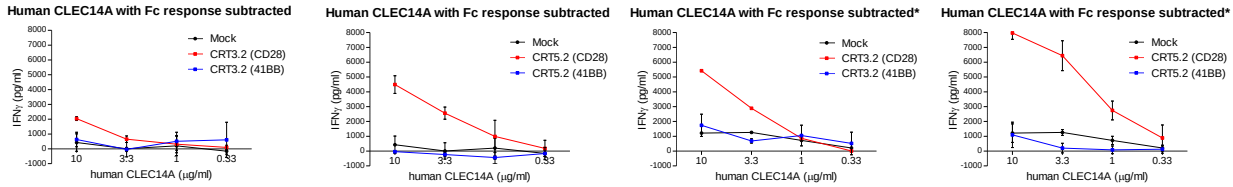

B

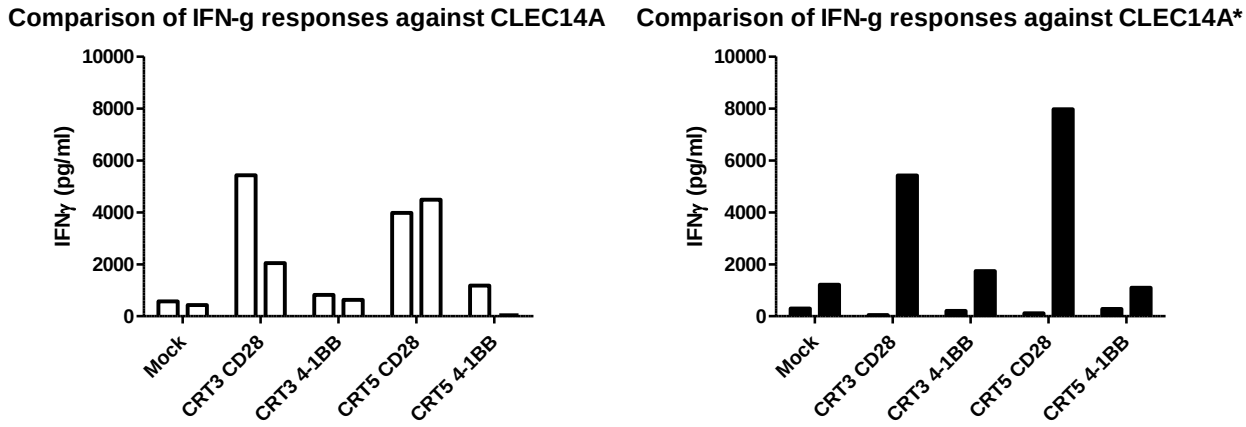

Figure 3.4 – IFN-γ response of transduced T cells in response to plate-bound human CLEC14A.

A – T cell IFN-γ production in response to a range of CLEC14A concentrations. Graphs show the IFN-γ production (in pg/ml) of each T cell line in response to CLEC14A concentrations from 10-0.33µg/ml as measured by sandwich ELISA. Plotted results show the specific IFN-γ response (response against CLEC14A-Fc with response against Fc alone subtracted). Red lines represent CD28-CAR^{+} T cells, blue lines represent 4-1BB-CAR^{+} T cells and black lines represent mock-transduced T cells. Error bars show standard deviations. Top panel shows the 1st experiment, while the bottom panel shows results from the 2nd experiment carried out (*=T cells have previously been cultured in human CLEC14A-Fc coated plates [right hand side]). **B – Comparison of maximal IFN-γ responses in transduced T cells.** Bar charts show the level of IFN-γ secretion in each T cell line at the highest CLEC14A-Fc concentration - 10µg/ml. As previously results displayed show the specific IFN-γ response with responses against Fc alone subtracted. Both repeats for each experiment are shown in grouped bars (black bars=previously cultured in CLEC14A-coated plates, white bars=cultured in standard tissue culture-treated plates).

(10μg/ml), but it appears that CRT5 CD28$^+$ T cells are able to produce IFN-γ in response to lower concentrations of CLEC14A (3.3-1μg/ml).

T cells that had been previously cultured on human CLEC14A-coated plates were also analysed for IFN-γ production (**Fig. 3.4A**). In the first ELISA, no responses were seen in any of the cells. The reasons for this are unknown, but the expected response was seen for the IFN-γ standards in this experiment. In the second ELISA, once again CD28-CAR $^+$ T cells produced more IFN-γ than the 4-1BB-CAR$^+$ T cells. Furthermore, CRT5 CD28$^+$ T cells produced higher levels of IFN-γ at every concentration of CLEC14A tested when compared to CRT3 CD28$^+$ T cells. Neither CRT3 4-1BB$^+$ T cells, or CRT5 4-1BB$^+$ T cells showed any IFN-γ response above background (mock-transduced T cell) levels. As expected, the highest magnitude of response was seen in cells that had previously been cultured in CLEC14A-coated plates (in CRT5-CD28$^+$ T cells) due to antigen specific cell expansion. Finally, the different T cell lines were also tested against mouse CLEC14A (**Fig. 3.5**). Surprisingly, no IFN-γ response was seen in any of the T cells studied, despite previous data from the lab and others indicating CAR-CD28$^+$ T cells produce IFN-γ in response to mouse CLEC14A [Steve Lee – personal communication]. This is most likely due to the batch of mouse CLEC14A, as no other experiments in the lab with this batch led to any IFN-γ production, whereas robust responses had been seen in experiments with previous batches [Steve Lee – personal communication].

These data are summed up in **Fig. 3.4B**. The maximal IFN-γ responses against human CLEC14A of the CD28-CAR$^+$ T cells are far greater than those of the 4-1BB-CAR$^+$ T cells, which themselves are no greater than the IFN-γ responses of mock-transduced T cells. No response against mouse CLEC14A was seen in these experiments.

Repeat 1:

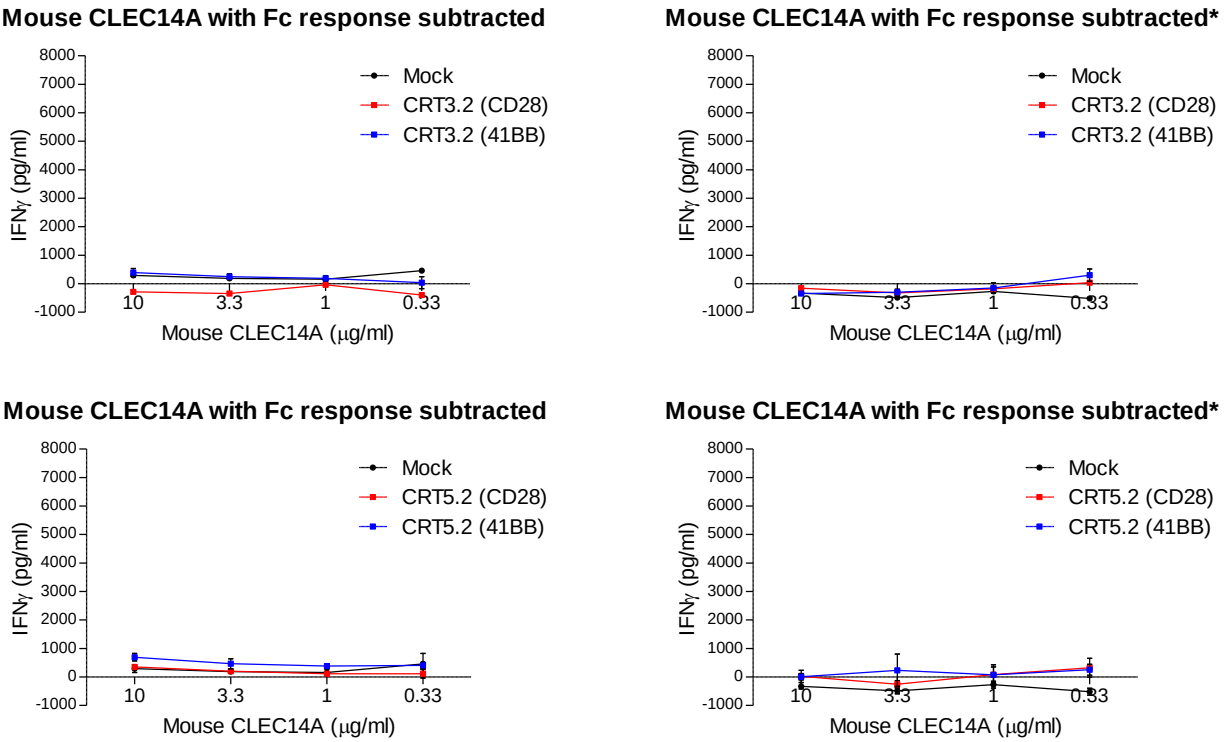

Figure 3.5 - IFN-γ response of transduced T cells in response to plate-bound mouse CLEC14A.

Graphs show IFN-γ production by T cells of each line against mouse CLEC14A-Fc concentrations of 10-0.33μg/ml. For key see figure 4A legend. Red lines represent CD28-CAR$^+$ T cells, blue lines represent 4-1BB-CAR$^+$ T cells and black lines represent mock-transduced T cells. Right panel (marked*) indicates T cells have previously been cultured on mouse CLEC14A-Fc coated plates.

3.4 – Enhanced cytotoxicity of T cells engineered to express CD28-CARs, compared to cells that express 4-1BB-CARs

Building on the previous IFN-γ response results, we next sought to investigate if there was any difference in antigen-specific cytotoxicity in T cells transduced with the CD28 or 4-1BB constructs. CD107a (also called lysosomal-associated membrane protein-1 [LAMP-1]) has been shown to be a reliable marker of induced T cell degranulation[45]. Therefore, we cultured T cells from each line with or without HUVEC cells (that naturally express CLEC14A[43]) and stained them for CD107a to monitor their cytotoxic activity.

Cells cultured in just media alone resulted in low percentages of CD107a staining, with a maximum level of 5.6% being observed (**Fig. 3.6B**). In the presence of HUVECs, CD28-CAR$^+$ T cells display a far superior degranulation response compared to T cells expressing 4-1BB-CARs. 4-1BB-CAR$^+$ T cells show negligible or no degranulation response above that of mock-transduced T cells. 4-1BB-CAR$^+$ T cell cytotoxicity is also not significantly increased in the presence of HUVECs. Taken together, these data show T cells expressing CD28-CARs are far superior at mediating an antigen-specific cytotoxic response when compared to 4-1BB-CARs.

3.5 – 4-1BB-CAR$^+$ T cells are more resistant to apoptosis than CD28-CAR$^+$ T cells, especially under hypoxic culture conditions

In vivo, many solid tumours develop a state of relative hypoxia compared to healthy tissue[46]. Therefore, for adoptive T cell therapies to be effective, the transferred T cells must be able to survive in hypoxic conditions. Some reports claim that T cells expressing CARs with 4-1BB costimulatory endodomains are more resistant to apoptosis than T cells expressing CARs with CD28 costimulatory endodomains [Carl

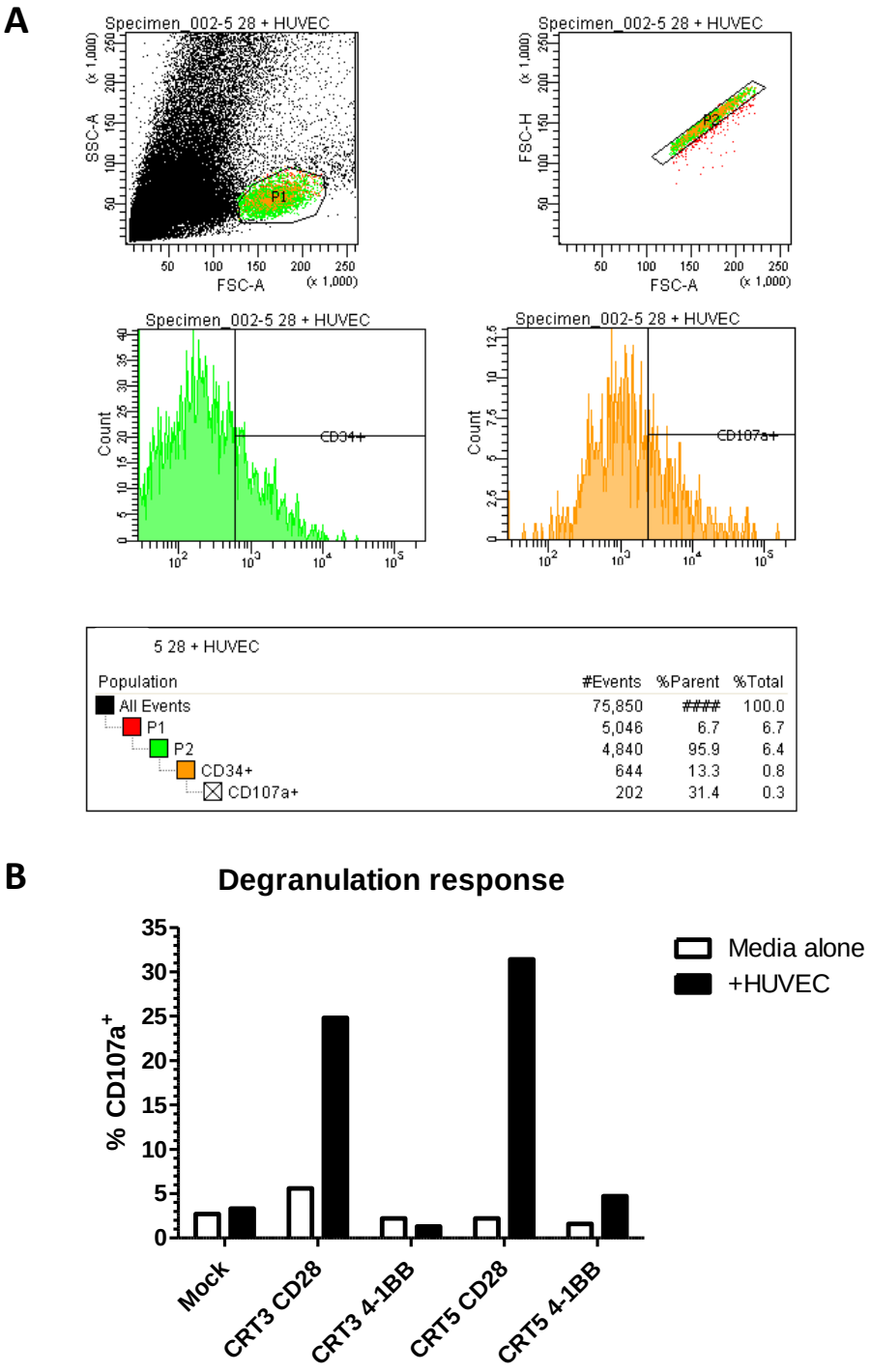

Figure 3.6 – Degranulation response of transduced T cell lines to natural CLEC14A-expressing HUVECs.

A – Gating strategy. First lymphocytes were gated on (P1), then singlet cells (P2). The $CD34^+$ fraction was determined and of these the percentage of $CD107a^+$ cells was calculated. Box illustrates gating hierarchy. **B – Degranulation response of the 4 different transduced T cell lines.** Bar chart shows response of the 4 lines and mock-transduced cells (n=1). Bar heights represent the percentage of $CD34^+$ singlet lymphocytes which are $CD107a^+$ (for mock-transduced cells bar heights represent the percentage of total singlet lymphocytes that are $CD107a^+$). Black and white bars signify T cells have been cultured with and without HUVECs respectively. These experiments used T cells that were previously cultured with human CLEC-14A-Fc.

June – personal communication]. To test this, cells were stained for the apoptosis marker Annexin V after culture in hypoxia or normoxia.

The first observation made was that as expected all cell lines (with the exception of mock-transduced controls) showed higher percentages of apoptosis at 1% O_2 than at normoxia (**Fig. 3.7B**). At normoxia, 4-1BB-CAR$^+$ T cells show marked resistance to apoptosis compared to mock-transduced T cells, and even more so compared to CD28-CAR$^+$ T cells. Similarly, under hypoxia the percentages of apoptotic cells were much lower in the 4-1BB-CAR$^+$ T cell lines than in the CD28-CAR$^+$ T cell line. Overall, CRT5$^+$ T cells appear better at resisting apoptosis than CRT3$^+$ T cells, with the CRT5-4-1BB construct performing best of all. Together these results agree with previous data, suggesting CARs with 4-1BB costimulatory endodomains allow for better T cell survival in both normoxia and hypoxia when compared to CARs with CD28 costimulatory endodomains.

A

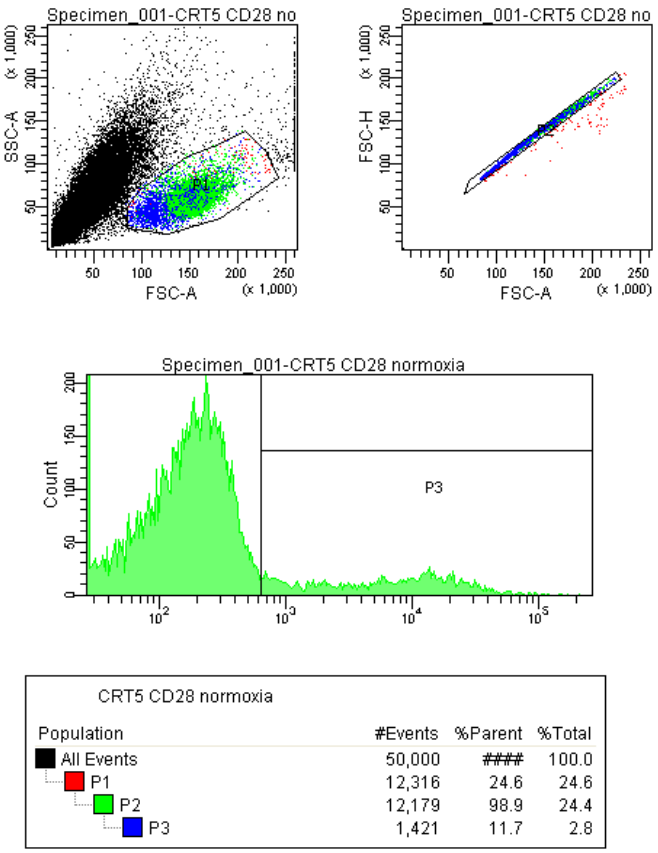

B **Apoptosis in response to hypoxia & normoxia**

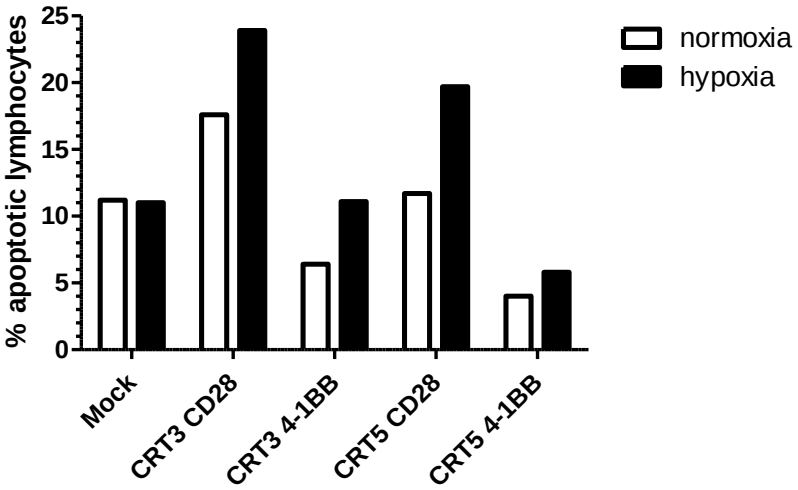

Figure 3.7 – Apoptosis in response to normoxia and hypoxia.

A – Gating strategy. Cells gated on lymphocytes first (P1), followed by single cells (P2) and finally Annexin V^+ apoptotic cells (P3). Box illustrates gating hierarchy. **B – Percentages of apoptotic cells in response to hypoxic/normoxic conditions.** Chart shows the percentage of lymphocytes that are apoptotic (Annexin V^+) in response to hypoxia (1% O_2 - black bars) or normoxia (21% O_2 - white bars)(n=1). These experiments used T cells that were previously cultured with human CLEC-14A-Fc.

4. DISCUSSION

2nd Generation CARs have shown promising early successes in phase 1 clinical trials in leukaemia. However, targeting solid tumours has proved to be a bigger challenge. Our lab uses a new approach; targeting tumour vasculature specifically through the C-type lectin CLEC14A. Building on successes using CARs containing CD28 costimulatory endodomains, this investigation aimed to compare this CAR to a new CAR containing a 4-1BB costimulatory endodomain.

Transduction efficiencies across the T cell lines were generally in the range of 10-20%. This is in line with what others in the lab achieve [Steve Lee – personal communication]. The mean percentages of CD28-CAR$^+$ T cells were slightly higher than those of the 4-1BB-CAR$^+$ T cells, but the results show that both CD28 and 4-1BB containing constructs can clearly be transduced into T cells. This bodes well for future experiments using 4-1BB-CAR constructs and indicates transfection and transduction methodology need not be altered. However, 4-1BB-CAR$^+$ T cells do not appear able to expand in response to plate-bound antigen in the same way as CD28-CAR$^+$ T cells can (based on three repeats – one representative example shown in **figure 3.2**). This could reflect possible differences in the abilities of 4-1BB and CD28 to activate T cells in response to antigen, but as human T cells are mostly memory cells, it would be expected 4-1BB would be better at inducing activation in response to antigen than CD28[29, 30].Needless to say this issue remains unresolved and needs further study.

Given the lack of clonal expansion seen by 4-1BB-CAR$^+$ T cells against CLEC14A, an associated trend would have also been expected in the proliferation assay experiment. However, little antigen-specific proliferation was seen in any of the 4 constructs. This is in disagreement with previous data that T cells with either

construct type can proliferate in response to antigen, with the response of CD28-CAR$^+$ T cells being stronger[17]. It is possible this discrepancy may be due to a degree of exhaustion or anergy due to overexposure to antigen or to the T cell mitogen IL-2 in our experiments. It is also possible the assay did not work if the T cells were in a poor condition which prevented any substantial proliferation *in vitro*. However, taking this data at face value, more generalised proliferation was seen in the cells expressing CD28-CARs. This fits with the fact that 4-1BB-CAR$^+$ T cells failed to expand to CLEC14A in plates previously, but is perhaps somewhat surprising given that 4-1BB signalling is thought to preferentially expand CD8$^+$ T cells[27]. CD8$^+$ T cells seemed to proliferate more than CD8$^-$ cells, but this was true for CD28-CAR$^+$ T cells as well as 4-1BB-CAR$^+$ T cells. More repeats of this assay need to be carried out (currently n=1) in order to understand these findings. Together the results suggest CD28-CARs transduce slightly better, and allow for more general proliferation of T cells when compared to 4-1BB-CARs.

Next the transduced T cells were analysed for the production of IFN-γ. When compared to 4-1BB-CAR$^+$ T cells, CD28-CAR$^+$ cells showed a far superior IFN-γ response to human CLEC14A. Against mouse CLEC14A, no response above background was seen in any T cell line. This may be due to the batch of mouse CLEC14A used, as others in the lab had been experiencing anomalous results with this batch. Future experiments with a new batch of mouse CLEC14A should produce an IFN-γ response from T cells, as others in the lab have shown previously with older batches [Steve Lee – personal communication]. Nonetheless, in the response against human CLEC14A, it is clear that CD28-constructs are favourable in inducing production of the inflammatory cytokine IFN-γ in T cells.

Concordantly, CD28-CAR$^+$ T cells also performed favourably in another test of T cell effector function – cytotoxicity. In the presence of CLEC14A expressing HUVECs, the degranulation response of T cells expressing the CD28-CARs were far greater than the minimal T degranulation response of T cells expressing 4-1BB-CARs. Although this is only from 1 repeat, the differences seen are substantial.

We also wanted to investigate levels of apoptosis in transduced T cells, including under hypoxic conditions, as *in vivo* many solid tumours exist in a state of hypoxia[46]. 4-1BB-CAR$^+$ T cells displayed reduced apoptosis in response to both normoxia and hypoxia compared to their CD28-CAR$^+$ T cell counterparts. This supports data from Carl June's lab at the University of Pennsylvania which suggested 4-1BB constructs mediate resistance to apoptosis to a greater degree than CD28 constructs [Carl June – personal communication]. As the level of mock-transduced cells lay intermediate to 4-1BB-CAR$^+$ T cells and CD28-CAR$^+$ T cells, it can also be inferred that CD28 constructs make T cells more susceptible to apoptosis, though the experiment needs repeating to be sure of this. This would make sense as CD28-CAR$^+$ T cells were shown to produce more IFN-γ and displayed a greater cytotoxic response, meaning these cells were more active than their 4-1BB-CAR$^+$ counterparts. Consequently, they could be subject to increased T cell exhaustion and apoptosis. Future studies looking at anergy and exhaustion markers such as programmed cell death-1 (PD-1), T-cell immunoglobulin domain and mucin domain 3 (TIM3) or lymphocyte-activation gene 3 (LAG-3) in the transduced T cells will help understand this further.

Taking the results together, it appears CD28-CAR$^+$ T cells transduce slightly better; and show enhanced *in vitro* IFN-γ and cytotoxic responses to antigen than 4-1BB-CARs. These data fit with previous reports that show IFN-γ production in CD28-CAR$^+$ T cells is higher[17], but disagree with others that claim 4-1BB$^+$ T cells produce more

IFN-γ[37]. Reasons for these differences could be due to different transduction methods (for example electroporation vs viral transduction), different assay methods and different antigen targets. Also, some data suggests 4-1BB constructs are better than CD28 constructs in clinical trials[39-41]. Differences observed in our study to these could include low repeat number, overstimulation of T cells in culture or the general shortcomings of *in vitro* cell culture models.

4-1BB constructs did allow for better survival, but this may also be due to lack of activation induced cell death and exhaustion as they are less active than cells transduced with CD28-CARs. As mentioned, it is possible T cell overactivation (resulting in anergy, exhaustion or apoptosis) could have played a big role in the outcome seen. Long term exposure to the T cell mitogen IL-2 and overstimulation with antigen could have resulted in this. Moreover, cells were kept in culture for up to three weeks. Towards the end of this period, cells may be less functionally active and comparisons became more difficult. Future experiments should therefore aim to culture cells for the minimum period possible. Nonetheless, CD28-CAR$^+$ T cells only showed a maximum of 25% apoptosis under hypoxia, indicating the majority still survive. Combined with the increased effector functions of these cells, these data alone would indicate CD28-CARs are the better option for further study into adoptive T cell transfer therapy for solid tumours, although more repeats of these data are clearly needed to back up these conclusions. An alternative option is to use 3rd generation CARs with both CD28 and 4-1BB costimulatory endodomains incorporated. Studies into such constructs are at an early stage, but are very promising; some suggesting enhanced proliferation, survival, cytokine production and tumour eradication *in vivo*[13, 37, 47].

Following on from this work, the two constructs could be compared *in vitro* in the following ways. Cytokine profiles could be studied by flow cytometry, and the production of these assayed in each cell line by ELISA methodology. These cytokines could include tumour necrosis factor-α, IL-2 and GM-CSF, similar to previous reports [17]. T cell subsets from each line could be analysed by flow cytometry. This could allow us to see if either construct resulted in a skewing towards specific T-helper subsets; or central or effector memory cells. Additionally, cloning work could be done to incorporate luciferase into these CARs. This would allow T cells expressing these constructs to be injected into cancerous mice and their migration patterns visualised by whole body intravital imaging. This way both CD28-CAR^+ T cells and 4-1BB-CAR^+ T cells could be compared directly for site specific cell migration and tumour size over time. Further work should be done to determine if CD28 constructs are also superior to 4-1BB constructs in terms of effector functions *in* vivo. Overall, based on these results CD28-CARs look a better option than 4-1BB CARs for adoptive immunotherapy targeting solid tumours. This work provides a platform for further research into the optimisation of adoptive therapies with CAR-expressing T cells as a feasible, robust treatment of human cancers.

References

1. Vesely, M. D., Kershaw, M. H., Schreiber, R. D. & Smyth, M. J. Natural Innate and Adaptive Immunity to Cancer. *Annu. Rev. Immunol.* **29**, 235-271 (2011).

2. Shankaran, V. *et al*. IFN gamma and lymphocytes prevent primary tumour development and shape tumour immunogenicity. *Nature* **410**, 1107-1111 (2001).

3. Svane, I. *et al*. Chemically induced sarcomas from nude mice are more immunogenic than similar sarcomas from congenic normal mice. *Eur. J. Immunol.* **26**, 1844-1850 (1996).

4. Engel, A., Svane, I., Rygaard, J. & Werdelin, O. MCA sarcomas induced in scid mice are more immunogenic than MCA sarcomas induced in congenic, immunocompetent mice. *Scand. J. Immunol.* **45**, 463-470 (1997).

5. Dunn, G., Old, L. & Schreiber, R. The three Es of cancer immunoediting. *Annu. Rev. Immunol.* **22**, 329-360 (2004).

6. Koebel, C. M. *et al*. Adaptive immunity maintains occult cancer in an equilibrium state. *Nature* **450**, 903-U24 (2007).

7. Girardi, M. *et al*. Regulation of cutaneous malignancy by gamma delta T cells. *Science* **294**, 605-609 (2001).

8. Restifo, N. P., Dudley, M. E. & Rosenberg, S. A. Adoptive immunotherapy for cancer: harnessing the T cell response. *Nat. Rev. Immunol.* **12**, 269-281 (2012).

9. Pardoll, D. & Topalian, S. The role of CD4(+) T cell responses in antitumor immunity. *Curr. Opin. Immunol.* **10**, 588-594 (1998).

10. Quezada, S. A. *et al*. Tumor-reactive CD4(+) T cells develop cytotoxic activity and eradicate large established melanoma after transfer into lymphopenic hosts. *J. Exp. Med.* **207**, 637-650 (2010).

11. Akhmetzyanova, I. *et al*. Tumor-specific CD4(+) T cells develop cytotoxic activity and eliminate virus-induced tumor cells in the absence of regulatory T cells. *Cancer Immunol. Immunother.* **62**, 257-271 (2013).

12. Kalos, M. & June, C. H. Adoptive T Cell Transfer for Cancer Immunotherapy in the Era of Synthetic Biology. *Immunity* **39**, 49-60 (2013).

13. Maus, M. V. *et al*. Adoptive immunotherapy for cancer or viruses. *Annu. Rev. Immunol.* **32**, 189-225 (2014).

14. Casucci, M. & Bondanza, A. Suicide Gene Therapy to Increase the Safety of Chimeric Antigen Receptor-Redirected T Lymphocytes. *J. Cancer* **2**, 378-382 (2011).

15. Savoldo, B. *et al*. CD28 costimulation improves expansion and persistence of chimeric antigen receptor-modified T cells in lymphoma patients. *J. Clin. Invest.* **121**, 1822-1826 (2011).

16. Carpenito, C. *et al*. Control of large, established tumor xenografts with genetically retargeted human T cells containing CD28 and CD137 domains. *Proc. Natl. Acad. Sci. U. S. A.* **106**, 3360-3365 (2009).

17. Finney, H., Akbar, A. & Lawson, A. Activation of resting human primary T cells with chimeric receptors: Costimulation from CD28, inducible costimulator, CD134, and CD137 in series with signals from the TCR zeta chain. *J. Immunol.* **172**, 104-113 (2004).

18. Zhong, X., Matsushita, M., Plotkin, J., Riviere, I. & Sadelain, M. Chimeric Antigen Receptors Combining 4-1BB and CD28 Signaling Domains Augment PI(3)kinase/AKT/Bcl-X-L Activation and CD8(+) T Cell-mediated Tumor Eradication. *Mol. Ther.* **18**, 413-420 (2010).

19. Sadelain, M., Brentjens, R. & Riviere, I. The Basic Principles of Chimeric Antigen Receptor Design. *Cancer Discov.* **3**, 388-398 (2013).

20. Kowolik, C. M. *et al*. CD28 costimulation provided through a CD19-specific chimeric antigen receptor enhances in vivo persistence and antitumor efficacy of adoptively transferred T cells. *Cancer Res.* **66**, 10995-11004 (2006).

21. Alegre, M., Frauwirth, K. & Thompson, C. T-cell regulation by CD28 and CTLA-4. *Nat. Rev. Immunol.* **1**, 220-228 (2001).

22. Vinay, D. & Kwon, B. Role of 4-1BB in immune responses. *Semin. Immunol.* **10**, 481-489 (1998).

23. Wen, T., Bukczynski, J. & Watts, T. 4-1BB ligand-mediated costimulation of human T cells induces CD4 and CD8 T cell expansion, cytokine production, and the development of cytolytic effector function. *J. Immunol.* **168**, 4897-4906 (2002).

24. DeBenedette, M., Shahinian, A., Mak, T. & Watts, T. Costimulation of CD28(-) T lymphocytes by 4-1BB ligand. *J. Immunol.* **158**, 551-559 (1997).

25. Hurtado, J., Kim, Y. & Kwon, B. Signals through 4-1BB are costimulatory to previously activated splenic T cells and inhibit activation-induced cell death. *J. Immunol.* **158**, 2600-2609 (1997).

26. Kim, Y., Kim, S., Mantel, P. & Kwon, B. Human 4-1BB regulates CD28 co-stimulation to promote Th1 cell responses. *Eur. J. Immunol.* **28**, 881-890 (1998).

27. HURTADO, J., KIM, S., POLLOK, K., LEE, Z. & KWON, B. Potential Role of 4-1bb in T-Cell Activation - Comparison with the Costimulatory Molecule Cd28. *J. Immunol.* **155**, 3360-3367 (1995).

28. Shuford, W. *et al*. 4-1BB costimulatory signals preferentially induce CD8(+) T cell proliferation and lead to the amplification in vivo of cytotoxic T cell responses. *J. Exp. Med.* **186**, 47-55 (1997).

29. GarniWagner, B. *et al*. 4-1BB is expressed on CD45RA(hi)RO(hi) transitional T cell in humans. *Cell. Immunol.* **169**, 91-98 (1996).

30. Pulle, G., Vidric, M. & Watts, T. IL-15-dependent induction of 4-1BB promotes antigen-independent CD8 memory T cell survival. *J. Immunol.* **176**, 2739-2748 (2006).

31. Melero, I. *et al*. Monoclonal antibodies against the 4-1BB T-cell activation molecule eradicate established tumors. *Nat. Med.* **3**, 682-685 (1997).

32. Miller, R. *et al*. 4-1BB-specific monoclonal antibody promotes the generation of tumor-specific immune responses by direct activation of CD8 T cells in a CD40-dependent manner. *J. Immunol.* **169**, 1792-1800 (2002).

33. Brentjens, R. J. *et al*. Genetically targeted T cells eradicate systemic acute lymphoblastic leukemia xenografts. *Clin. Cancer Res.* **13**, 5426-5435 (2007).

34. Maher, J. Immunotherapy of malignant disease using chimeric antigen receptor engrafted T cells. *ISRN oncology* **2012**, 278093 (2012).

35. Kochenderfer, J. N. *et al*. B-cell depletion and remissions of malignancy along with cytokine-associated toxicity in a clinical trial of anti-CD19 chimeric-antigen-receptor-transduced T cells. *Blood* **119**, 2709-2720 (2012).

36. Davila, M. L. Efficacy and Toxicity Management of 19-28z CAR T Cell Therapy in B Cell Acute Lymphoblastic Leukemia. *Sci. Transl. Med.* **6**, 224ra25 (2014).

37. Zhong, X., Matsushita, M., Plotkin, J., Riviere, I. & Sadelain, M. Chimeric Antigen Receptors Combining 4-1BB and CD28 Signaling Domains Augment PI(3)kinase/AKT/Bcl-X-L Activation and CD8(+) T Cell-mediated Tumor Eradication. *Mol. Ther.* **18**, 413-420 (2010).

38. Milone, M. C. *et al*. Chimeric Receptors Containing CD137 Signal Transduction Domains Mediate Enhanced Survival of T Cells and Increased Antileukemic Efficacy In Vivo. *Mol. Ther.* **17**, 1453-1464 (2009).

39. Porter, D. L., Levine, B. L., Kalos, M., Bagg, A. & June, C. H. Chimeric Antigen Receptor-Modified T Cells in Chronic Lymphoid Leukemia. *N. Engl. J. Med.* **365**, 725-733 (2011).

40. Porter, D. L., Kalos, M., Zheng, Z., Levine, B. & June, C. Chimeric Antigen Receptor Therapy for B-cell Malignancies. *J. Cancer* **2**, 331-332 (2011).

41. Kalos, M. *et al*. T Cells with Chimeric Antigen Receptors Have Potent Antitumor Effects and Can Establish Memory in Patients with Advanced Leukemia. *Sci. Transl. Med.* **3**, 95ra73 (2011).

42. Barrett, D. M., Singh, N., Porter, D. L., Grupp, S. A. & June, C. H. Chimeric antigen receptor therapy for cancer. *Annu. Rev. Med.* **65**, 333-347 (2014).

43. Mura, M. *et al*. Identification and angiogenic role of the novel tumor endothelial marker CLEC14A. *Oncogene* **31**, 293-305 (2012).

44. Schoenborn, J. R. & Wilson, C. B. Regulation of interferon-gamma during innate and adaptive immune responses. *Adv. Immunol.* **96**, 41-101 (2007).

45. Betts, M. *et al*. Sensitive and viable identification of antigen-specific CD8+T cells by a flow cytometric assay for degranulation. *J. Immunol. Methods* **281**, 65-78 (2003).

46. Brown, J. M. Tumor hypoxia in cancer therapy. *Methods Enzymol.* **435**, 297-+ (2007).

47. Carpenito, C. *et al*. Control of large, established tumor xenografts with genetically retargeted human T cells containing CD28 and CD137 domains. *Proc. Natl. Acad. Sci. U. S. A.* **106**, 3360-3365 (2009).